Thermal Science and Engineering Progress 50 (2024) 102460

Contents lists available at ScienceDirect

Thermal Science and Engineering Progress

journal homepage: www.sciencedirect.com/journal/thermal-science-and-engineering-progress

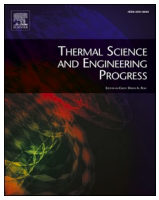

# Lattice Boltzmann modeling of buoyant convection in an enclosure with differentially heated porous cylinders

B. Shruti, S. Dhinakaran *

*The Centre for Fluid Dynamics, Department of Mechanical Engineering, Indian Institute of Technology Indore, Simrol, Indore 453 552, India*

ARTICLE INFO

*Keywords:*
Porous media
Natural convection
Lattice Boltzmann method
Darcy-Brinkman-Forchheimer model
Differentially heated cylinders
Enclosure

ABSTRACT

This study employs the Lattice Boltzmann Method, utilizing the Darcy-Brinkmann-Forchheimer model, to investigate buoyancy-driven heat transfer within an enclosure featuring differentially heated porous cylinders. The enclosure comprises two isothermal cylinders (one hot and one cold) separated by a distance within a cooled enclosure. It comprehensively assesses the impact of Darcy numbers ranging from $10^{-6}$ to $10^{-2}$, Rayleigh numbers spanning from $10^{4}$ to $10^{6}$, and various cylinder orientations. Specifically, five distinct configurations are considered, including horizontal alignment of hot and cold cylinders (Case A), vertical alignment of hot and cold cylinders (Cases B & C), and diagonal alignment of hot and cold cylinders (Cases D & E). The key findings highlight that the highest heat dissipation occurs in proximity to the heated cylinder, with certain orientations consistently demonstrating superior heat dissipation. The study explores the heat and flow characteristics at different Rayleigh numbers, examining these through streamlines and isotherms. Also, the impact of cylinder permeability on heat transfer features is comprehensively analyzed and reported. The findings of this research offer valuable insights for optimizing the placement of electronic components within compact electronic cabinets, with potential benefits for electronic cooling and thermal management.

## Introduction

Heat transfer via buoyant forces inside enclosures has been a key topic of research for decades, yet it still has practical uses, such as the cooling of electronic components. In the period of industrialization, technology is expanding rapidly. In today's technological environment, electronic equipment is indispensable. Continuous use of equipment generates heat, raising the temperature of electrical components. To ensure proper operation, their temperature must be maintained. Due to industry's need for a low-maintenance and cost-effective method of heat transfer, extensive research is conducted in this field.

Natural convection is a buoyancy-induced phenomenon in which density fluctuations cause heat transfer, requiring no additional methods of heat removal. This investigation focuses on buoyancy-induced heat transfer from a heated porous cylinder to a cold one. Flow and heat transfer depend on convection through and around the porous cylinders differentially heated within a closed enclosure. The excellent cooling characteristics of porous media are well-known [1] and this research aims to enhance the heat transfer method by reconfiguring the hot and cold cylinders. By examining the intricate interaction between these heated and cold porous cylinders within an enclosed environment, one can gain valuable insights into the nuances of heat transfer characteristics. Consequently, several researchers are examining this subject.

Bhattacharyya et al. [2] performed numerical investigation around and through a porous cylinder. The Brinkman, Forcheimmer and nonlinear convective terms were considered for a permeable body. The study states, as the Darcy number increases, the drag coefficient, wake length, and separation angle decreases. Yoon et al. [3] examined free convection in an enclosure with cold walls and two heated cylinders. The authors explored the effects of cylinder radius (ranging from 0.05L to 0.2L). As the cylinder radius increased, the surface mean Nusselt number on each enclosure wall also increased. When *Ra* reached $10^{5}$, reducing the cylinder radius caused a disruption in the symmetry inside the enclosure. Moukalled and Acharya [4] conducted a heat transfer study caused by natural convection on a circular cylinder that was uniformly heated. They examined different aspect ratios (R/L = 0.1–0.3). If the size is larger, two opposing effects can be seen. The heat transfer rate enhances along with buoyancy induced convection due to greater surface area but consequently leads to viscous retardation. This results in reduction of fluid velocity.

* Corresponding author.
*E-mail address:* sdhina@iiti.ac.in (S. Dhinakaran).

https://doi.org/10.1016/j.tsep.2024.102460
Received 26 September 2023; Received in revised form 17 December 2023; Accepted 12 February 2024
Available online 15 February 2024

**Nomenclature**

*Notations*

| | |
|---|---|
| $C_1$, $C_2$ | Binary constants |
| $c_F$ | Non-dimensional Forchheimer term |
| $c_s$ | Speed of sound [$ms^{-1}$] |
| $Da$ | Darcy number $\frac{K}{D^2}$ |
| $d_p$ | Particle diameter [m] |
| $e_i$ | Discrete lattice velocity in direction $i$, $\frac{\Delta x_i}{\Delta t}$ |
| $F$ | Body force due to presence of the porous medium [N] |
| $F_i$ | Total force term due to porous medium [N] |
| $F_b$ | Boussinesq force term [N] |
| g | Gravitational acceleration [$ms^{-2}$] |
| $f_i$ | Particle distribution function along $i^{th}$ link direction |
| $f_i^{eq}$ | Equilibrium distribution function along $i^{th}$ link direction |
| $g_i$ | Temperature distribution function along $i^{th}$ link direction |
| $g_i^{eq}$ | Equilibrium distribution function of temperature $i^{th}$ link direction |
| $L$ | Length of enclosure [m] |
| $\tau_t$ | Non-dimensional time $\frac{t*u_o}{H}$ |

*Greek symbols*

| | |
|---|---|
| $\rho$ | Fluid density [$kg.m^{-3}$] |
| $\tau$ | Dimensionless relaxation time for density |
| $\tau'$ | Dimensionless relaxation time for temperature |
| $\Delta t$ | Time step [$s$] |
| $\Delta x$ | Lattice space |
| $\theta$ | Dimensionless temperature $\frac{T-T_\infty}{T_w-T_\infty}$ |
| $\sigma$ | Thermal Conductivity ratio |

*Subscripts*

| | |
|---|---|
| avg | Average |
| $i$ | Lattice link direction |
| M | Mean value |
| ° | Initial value |

*Superscripts*

| | |
|---|---|
| * | Dimensional form of variables |
| $D$ | Diameter of Cylinder [m] |
| $\delta$ | Distance from centre ($\delta x$ or $\delta y$ in $x$ and $y$ direction) |
| G | Body force due to gravity [N] |
| $N$ | Number of lattices on the cylinder |
| $Nu_l$ | Local Nusselt number $\frac{\partial\theta}{\partial n}$ |
| $Nu$ | Nusselt number $\frac{hL}{K}$ |
| $Nu_{avg}$ | Average Nusselt number |
| $P$ | Dimensionless pressure $\frac{p^*}{\rho u_\infty^2}$ |
| $Pr$ | Prandtl number $\frac{\nu}{\alpha}$ |
| $Ra$ | Rayleigh number $\frac{g\beta\Delta TL^3}{\alpha\nu}$ |
| $u$ | Non-dimensional $x$-component velocity [$ms^{-1}$] |
| $v$ | Non-dimensional $y$-component velocity [$ms^{-1}$] |
| U | Actual velocity [$ms^{-1}$] |
| V | Auxiliary velocity [$ms^{-1}$] |
| $w_i$ | Weighing factor in direction $i$ |
| $x,y$ | Non-dimensional horizontal & vertical coordinate |
| $x^*,y^*$ | Dimensional horizontal & vertical coordinate |
| $\epsilon$ | Porosity |
| $\nu$ | Fluid kinematic viscosity [$m^2s^{-1}$] |
| $\mu$ | Fluid dynamic viscosity [$Nsm^{-2}$] |
| $\Lambda$ | Viscosity ratio, $\frac{\mu_e}{\mu}$ |
| $\alpha$ | Thermal diffusivity [$m^2s^{-1}$] |
| $\beta$ | Thermal Expansion Coefficient $\frac{Ra\alpha\nu}{g\Delta TL^3}$ [$K^{-1}$] |
| w | Wall |
| e | Effective |
| f | Fluid |

Furthermore, Yoon et al. [5] investigated heat transfer using hot and cold solid cylinders within cooled enclosures through computational methods. The results demonstrate that positioning the heated cylinder below and the cold cylinder above increases the space available for upward heat transfer. When the cylinder radius is 0.05L, convection effects become more pronounced, whereas with a radius of 0.2L, conduction effects become prominent. Shruti et al. [6] conducted a numerical investigation of natural convection within an enclosure containing a porous cylinder. They altered the cylinder's position to the top, centre, bottom, right, bottom-diagonal, and top-diagonal locations, respectively. Their findings revealed that the most efficient heat conduction occurred when the cylinders were positioned in the bottom-diagonal configuration. Ho et al. [7] studied heat transfer from an adiabatic circular enclosure with two differently heated cylinders. They examined the effects of changing the Rayleigh number from $10^4$ to $10^7$, varying the inclination angle relative to gravity at 30, 60, and 90 degrees, and adjusting the distance between cylinders ($s/d = 0.7$, 0.8333, and 1.0). These factors significantly influence the heat transfer characteristics. With the exception of the vertical orientation, the heat exchange between cold and hot cylinders is primarily governed by fluid recirculation in the counterclockwise direction for all orientations tested.

Another follow-up study by Ho et al. [8] analyzed the effect of hot and cold cylinders inside circular-shaped enclosures exposed to ambient temperature. Convection from the enclosure wall to the atmosphere adds to the buoyant forces generated between the cylinders, accelerating total heat transfer. Baranwal et al. [9] investigated the effects of yield stress on natural convection. The hot and cold cylinders are arranged side by side, and the enclosure is filled with Bingham plastic fluid. They studied the effects of the Prandtl number (ranging from 10 to 100), Rayleigh number (ranging from $10^2$ to $10^6$), and Bingham number (ranging from 0.01 to 100). The cylinder's location from the centre is varied as 0, 0.1, 0.2, and 0.25. A decrease in the $Nu_{avg}$ value is observed with increasing Prandtl and Bingham numbers. Heat transfer is enhanced when cylinders are positioned beneath the horizontal centerline of the enclosure. At $Bn/Gr = 0.01$, convection occurs. For large Bingham numbers, $Nu_{avg}$ reaches an asymptotic value, indicating that heat transfer occurs primarily through conduction.

Mishra et al. [10] investigated heat transfer by free convection generated by differentially heated cylinders positioned both vertically and diagonally in closed chambers filled with Bingham plastic fluid. They examined the effect of the Prandtl number (ranging from 10 to 100), Rayleigh number (ranging from $10^4$ to $10^6$), Bingham number (ranging from 0.01 to $Bn_{max}$), cylinder location, and spacing between them in the vertical (ranging from 0 to 0.25) and diagonal (ranging from 0.15 to 0.35) orientations. Moving the cylinders away from the vertical centerline marginally reduces the $Nu_{avg}$ of the heated cylinder, while placing them closer to the enclosure's sides increases it. In cases where cylinders are arranged diagonally, increasing the distance between them reduces the $Nu_{avg}$ value.

Corcione et al. [11] conducted a numerical study involving differentially heated cylinders within an inclined cavity containing alumina/water nanofluid. The variables considered included the nanoparticles' volume percentage (ranging from 0 to 0.04), the angle of inclination (ranging from 0° to 70°), nanoparticle diameter (ranging from 25 nm to 75 nm), nanofluid temperature (ranging from 300 K to 330 K), and the

distance between cylinders (ranging from 0.3 to 0.6). According to their findings, at a tilting angle of 70 degrees, buoyant forces create high-concentration space above low-concentration space. Also, the temperature differential between the cylinders generates a thermal driving force, contributing to oscillatory flow. Ma et al. [12] conducted a numerical analysis of the angle effect between differentially heated cylinders placed between two coaxial adiabatic cylinders filled with nanofluids (Cu-Ethylene Glycol, Cu-Water, and Cu-Water/Ethylene Glycol). The investigation involved one heated cylinder and one, two, and three cold cylinders positioned at various angles, ranging from 0° to 315°, with $Ra$ varying from $10^3$ to $10^5$. The configuration with two cylinders positioned at 30 degrees, or in the case of three cylinders, a heated cylinder at the bottom and two cold cylinders at 90 degrees and 180 degrees, exhibited the highest $Nu_{avg}$ value. The arrangement with four cylinders, with the heated one at 0° and cold cylinders at 90°, 180°, and 270°, achieved the maximum $Nu_{avg}$ value.

Ho et al. [13] conducted a further analysis of transient natural convection in a circular enclosure, revealing periodic variations with distinct patterns. At $Ra = 6 \times 10^5$, the flow direction shifts from clockwise to anticlockwise, while at $Ra = 1.2 \times 10^6$, the strength of the flow field transitions from strong to weak. Garoosi et al. [14] performed a numerical analysis of nanofluid-filled square, circular, and triangular enclosures. Within a thermally insulated enclosure, they analyzed the orientation, shape (circle and ellipse), and quantity of cold and hot cylinders. For low $Ra$ values, the findings suggest that changing the enclosure shape from square to triangular leads to a decrease in the heat transfer rate. Positioning the cylinders vertically results in a higher heat transfer rate. At $Ra = 10^5$, increasing the number of cylinder pairs has little effect on $Nu_{avg}$.

Quintino et al. [15] analyzed a nanofluid-filled (CuO, $Al_2O_3$, $TiO_2$ with $H_2O$ as the base fluid) adiabatic enclosure with differentially heated cylinders. Using a double-diffusive method with a two-phase model, they observed that an increase in temperature significantly increases the dispersion of nanoparticles in the base fluid. As the size of nanoparticles decreases, the width of the cavity expands, and the temperature difference between the cylinders increases, leading to a substantial increase in dispersion. Quintino et al. [16] extended this investigation to explore the effects of sloping adiabatic cavities. An increase in the tilting angle from 0° to 60° enhances the solute driving force and velocity of the fluid, thereby improving heat transfer. Garoosi et al. [17] conducted a computational investigation of natural and mixed convection inside rectangular and square adiabatic enclosures. They analyzed the impact of orientation, size, quantity, and shape (circle and ellipse) of cooled and heated cylinders, demonstrating a significant influence on heat transport. The addition of cold cylinders at a high Rayleigh number increases heat transfer rates, but for $Ra = 10^5$, the opposite trend is observed.

Garoosi et al. [18] conducted additional research on an elliptical adiabatic enclosure incorporating nanofluid-filled cylinders with differential heating. Shifting the heated cylinder's location from the bottom to the top inhibits heat transfer. The horizontal configuration with $Ra = 10^4$ provides a better rate of heat dissipation. However, when the $Ra$ value is increased, the opposite effect is observed. Nithiarasu et al. [19] conducted numerical work on a porous enclosure with differentially heated walls, considering Rayleigh numbers ranging from $10^3$ to $5 \times 10^9$. The porous medium layer has an impact on the flow and thermal field, which enhances heat dissipation from the enclosure. Mishra et al. [20] conducted a numerical investigation using differentially heated cylinders oriented both vertically and horizontally within an enclosure containing fluids governed by the power law. The cylinder's location varied for $Gr$ ranging from $10^2$ to $10^4$, power-law index ranging from 0.2 to 2, and $Pr$ ranging from 0.7 to 100. An asymmetrical arrangement of cylinders was found to optimise heat transfer, with the horizontal arrangement providing superior heat transfer compared to the vertical and diagonal configurations.

Ho et al. [21] investigated transient natural convection inside an adiabatic circular cylinder, exploring the position and distance between differentially heated cylinders. In the case of vertically aligned cylinders, an increase in Rayleigh number and a decrease in cylinder distance lead to transient changes in hydrothermal properties. Hu and Mei [22] investigated heat transfer in a rectangular enclosure connected to a permeable wall. An increase in the Darcy number resulted in a 90 % increase in $Nu_{avg}$. However, a thicker porous wall reduced heat transfer efficiency by 50 %. Moreover, tilting the enclosure to a 90° angle resulted in a minimum heat transfer rate. Nammi et al. [23] conducted a numerical analysis using four solid heated cylinders placed within a porous confinement. The Darcy number ranged from $10^{-4}$ to $10^{-2}$, the Rayleigh number ranged from $10^3$ to $10^6$, and the spacing between the cylinders ranged from 0.3 to 0.6. At $Da = 10^{-3}$, the time-averaged Nusselt number of the lower cylinders initially decreased between 0.3 and 0.4 and then subsequently rose to 0.6.

The literature review presents studies involving various sizes of solid cylinders ranging from $R = 0.1$L-0.4L with one cylinder and two cylinders $R = 0.05\text{L} - 0.2\text{L}$. According to the literature, the size and position of cylinders have a significant influence on heat transfer rates [3–6]. If the size is larger, two opposing effects can be observed. The heat transfer rate enhances along with buoyancy induced convection due to greater surface area, but this consequently leads to viscous retardation. As a result, there is a reduction in fluid velocity [4]. Within the lower radius range, the effect of convection on increasing the Nusselt number of the upper cylinder exceeds that of conduction in the enclosure with two cylinders. However, when the radius increases, the conduction in the region between two cylinders becomes more prominent compared to convection [3]. Overall, the literature review underscores the critical influence of solid cylinder size and position on heat transfer rates and therefore it is important to study the size as well as position effects.

There have been numerous numerical studies reported in the literature on differentially heated solid cylinders in natural convection within an enclosure. Due to increased buoyancy, thermal plumes from the hot cylinder easily impact the cold cylinder. Heat exchange occurs both within the cylinders and with the enclosure walls. The porous media expands the area available for fluid circulation within the container. The combination of permeable and cold cylinders promotes natural convection processes.

To the best of the authors' knowledge, no studies have been conducted on the effects of the position of differentially heated porous circular cylinders inside a cooled enclosure on natural convection. The aim of this investigation is to fill that gap. The main objective is to examine how several factors, including cylinder position, Darcy number, and Rayleigh number, affect flow and heat transfer. This research also enables the optimal positioning of heated and cooled porous cylinders within an enclosure to maximize heat dissipation. The novel aspect of this research lies in its applicability to passive cooling of electronic cabinets, and other systems. Furthermore, these numerical analyses help clarify how hot and cold porous cylinders interact with the enclosure wall.

## Physical model and numerical methodology

### *Problem definition and geometrical setup*

Porous cylinders, one hot and one cold, are placed inside a square enclosure with cold walls. These cylinders are oriented in various ways, including vertically, horizontally, and diagonally. The study examines the influence of parameters such as the Rayleigh number (ranging from $10^4$ to $10^6$) and the Darcy number (ranging from $10^{-6}$ to $10^{-2}$) on the heat transfer rates

The enclosure is filled with air, and the cylinder's radius is $R = 0.1L$, with a distance of $0.5L$ between the centers of the cylinders, as depicted in Fig. 1. The locations of the heated and cold cylinders are varied from top to bottom vertically and diagonally. However, the variation in the cylinder's position from left to right does not affect the results and,

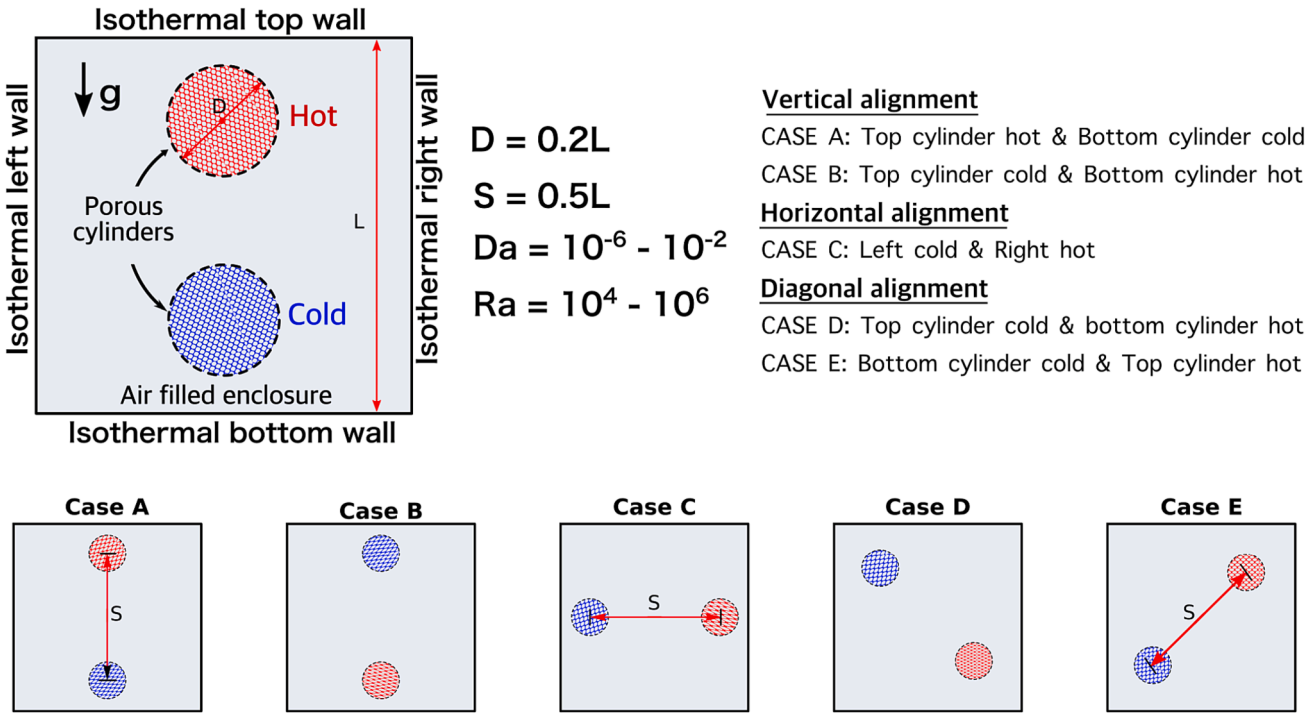


**Fig. 1.** Schematic diagram illustrating natural convection heat transfer from differentially heated porous cylinders within an enclosure.

therefore, was not studied. Following are the different cylinder arrangements considered in this study (the $x$ and $y$ coordinates are provided in brackets):

- Case A - Hot upper cylinder (0.5L, 0.75L) & cold lower cylinder (0.5L, 0.25L)
- Case B - Cold upper cylinder (0.5L, 0.75L) & hot lower cylinder (0.5L, 0.25L)
- Case C - Hot left cylinder (0.25L, 0.5L) & Right Cold cylinder (0.75L, 0.5L)
- Case D - Cold upper-diagonal (0.324L, 0.678L) & Hot lower-diagonal (0.68L, 0.32L)
- Case E - Hot upper-diagonal (0.68L, 0.68L) & Cold lower-diagonal (0.32L, 0.32L)

The assumptions used in the study are as follows:

- Air is the working fluid, exhibiting Newtonian behaviour with constant properties.
- The fluid is incompressible and flows two-dimensionally in a steady regime.
- Radiation from the heated cylinders is considered negligible.
- The porous media and fluid are in thermal equilibrium, resulting in a thermal conductivity ratio of one between the fluid and porous material.
- A single-phase fluid flows through a porous region consisting of a homogeneous and isotropic medium.
- The values of porosity and permeability remain uniform throughout the region

*Governing equations*

The Darcy-Brinkman-Forchheimer model and the modified energy equation are employed to model flow and heat transfer through porous media. These equations are presented in non-dimensional form for simulating buoyancy-induced convection through porous bodies and are given as [19].

$$\frac{\partial u}{\partial x}+\frac{\partial v}{\partial y}=0 \tag{1}$$

$$\frac{1}{\epsilon}\frac{\partial u}{\partial \tau_t}+\frac{1}{\epsilon^2}\left(u\frac{\partial u}{\partial x}+v\frac{\partial u}{\partial y}\right)=-\frac{\partial p}{\partial x}+\frac{Pr}{\epsilon}\left(\frac{\partial^2 u}{\partial x^2}+\frac{\partial^2 u}{\partial y^2}\right)-C_1\frac{Pr}{Da}u -C_2\frac{1.75}{\sqrt{150}}\frac{1}{\sqrt{Da}}\times\frac{\sqrt{u^2+v^2}}{\epsilon^{3/2}}u \tag{2}$$

$$\frac{1}{\epsilon}\frac{\partial v}{\partial \tau_t}+\frac{1}{\epsilon^2}\left(u\frac{\partial v}{\partial x}+v\frac{\partial v}{\partial y}\right)=-\frac{\partial p}{\partial y}+\frac{Pr}{\epsilon}\left(\frac{\partial^2 v}{\partial x^2}+\frac{\partial^2 v}{\partial y^2}\right)-C_1\frac{Pr}{Da}v -C_2\frac{1.75}{\sqrt{150}}\frac{1}{\sqrt{Da}}\times\frac{\sqrt{u^2+v^2}}{\epsilon^{3/2}}v+Ra\,Pr\,\theta \tag{3}$$

$$\sigma\frac{\partial \theta}{\partial \tau_t}+\left(u\frac{\partial \theta}{\partial x}+v\frac{\partial \theta}{\partial y}\right)=\frac{k_{eff}}{k_f}\left(\frac{\partial^2 \theta}{\partial x^2}+\frac{\partial^2 \theta}{\partial y^2}\right) \tag{4}$$

In the non-porous region, we apply the continuity, Navier-Stokes, and energy equations. In equation (3), binary constants $C_1$ and $C_2$ are specified as having a value of zero in the clear fluid region and a value of one for the porous region. The Prandtl number is defined as $Pr = \mu\, c_p/k_f$. The effective thermal conductivity is expressed as:

$$k_{eff}=\epsilon k_f+(1-\epsilon)k_s \tag{5}$$

Here, the thermal conductivity of fluid ($k_f$) as well as porous medium ($k_s$) is assumed to be the same. Therefore, the ratio of thermal conductivity ($\sigma$) is unity, representing non-homogeneous variation in porosity [19].

The characteristic scales assumed for dimensionless governing equations are defined as follows:

$$x=\frac{x^*}{L},\ y=\frac{y^*}{L},\ \tau_t=\frac{tu_o}{L},\ p=\frac{p^*L^2}{\rho\alpha^2},\ u=\frac{u^*L}{\alpha},\ v=\frac{v^*L}{\alpha},\ \theta=\frac{T-T_c}{T_h-T_c} \tag{6}$$

The dimensional quantities are denoted by the superscript *.

*Lattice Boltzmann method*

The theory of Lattice Gas Automata implemented on a meso scale is known as the Lattice Boltzmann Method (LBM). This approach finds its origins in the kinetic Boltzmann equation. In LBM equations, the convective terms of the Navier-Stokes equation are nonlinear, while the linear terms are well-defined. Particles are assumed to be situated on a lattice grid and undergo collision and streaming as they move in various directions. These particles subsequently collide with particles from another lattice, a process referred to as the collision step, and then move to another adjacent lattice in the streaming step.

In LBM, calculations are carried out using probability distribution functions denoted as '$f$' for the velocity field and '$g$' for the temperature field. The governing parameters for fluid flow are the kinematic viscosity and thermal diffusivity for thermal fields. Furthermore, the values of density, velocity, and temperature are determined in terms of LBM units through the following equations.

*Equation for flow field*

The first step in LBM is the collision process, where a particle from one lattice collides with the particle on the next lattice. The equation for calculating the distribution function for the flow field '$f_i$' through the collision process is expressed as [24]:

$$f_i(x+e_i\Delta t, t+\Delta t) - f_i(x,t) = -\frac{1}{\tau}[f_i(x,t) - f_i^{eq}(x,t)] + \Delta t F_b + \Delta t F_i \tag{7}$$

In this equation, '$e_i$' denotes the direction and magnitude of velocity, '$\tau$' is the relaxation factor, $f_i$ is the instantaneous distribution function, '$f_i^{eq}$' is the corresponding particle distribution function, and the additional forces are computed in terms of '$F_b$' for free convection effects due to buoyant forces and $F_i$ accounts for drag forces arising from porous media.

The two-dimensional analysis is done using the $D_2Q_9$ model (as shown in Fig. 2). The particles stream in nine directions with different speeds, and the computation of particle speed is performed with the following equations:

$$e_i = \begin{cases} (0,0), & i = 0 \\ (cos[(i-1)\pi/2], sin[(i-1)\pi/2])e, & i = 1-4 \\ (cos[(2i-9)\pi/4], sin[(2i-9)\pi/4])\sqrt{2e}, & i = 5-8 \end{cases} \tag{8}$$

In eq. (7), the first term of the right side represents the calculation of the BGK collision operator value using the Single Relaxation Time model (SRT). As particles tends to relax toward equilibrium, relaxation factor ($\tau$) is determined at each collision step. In this context, all particles within the lattice share the same value for $\tau$. The relationship between dimensionless relaxation time and fluid viscosity in terms of Lattice Boltzmann (LB) units is defined by Chapman-Enskog equation, expressed as:

$$\boldsymbol{\nu} = \left(\boldsymbol{\tau} - \frac{1}{2}\right)\Delta t\, \boldsymbol{c}_s^2 \tag{9}$$

Here, '$c_s$' represents the speed of sound, defined as $\frac{c_k}{\sqrt{3}}$ ($\boldsymbol{c}_k$ is the unit vector) in the $D_2Q_9$ model.

The force term '$F_i$', computes the drag effects generated by permeable materials when fluid flows through them. Consequently, it is specifically computed within the porous region, assigned a zero value in the fluid region. The equation is written as:

$$F_i = w_i\rho\left(1 - \frac{1}{2\tau}\right)\left[3(e_i{\cdot}F) + \frac{9}{\epsilon}(e_i{\cdot}U)(e_i{\cdot}F) - \frac{3}{\epsilon}(U{\cdot}F)\right] \tag{10}$$

The Darcy-Forchheimer Force term, resulting from the porous body, is defined by the following expression. This force encompasses both the viscous and inertial effects:

$$F = -\frac{\epsilon\nu}{K}U - \frac{\epsilon c_F}{\sqrt{K}}|U|U + \epsilon G \tag{11}$$

The equilibrium distribution function, denoted as '$f_i^{eq}$' is expressed as:

$$f_i^{eq} = w_i\rho[1 + 3(e_i{\cdot}U) + \frac{9}{2\epsilon}(e_i{\cdot}U)^2 - \frac{3}{2\epsilon}(U{\cdot}U)] \tag{12}$$

The density is calculated by the summation of the distribution function, while the velocity generated due to porous media is termed as the auxiliary velocity, denoted as $V$ in Eq (14).

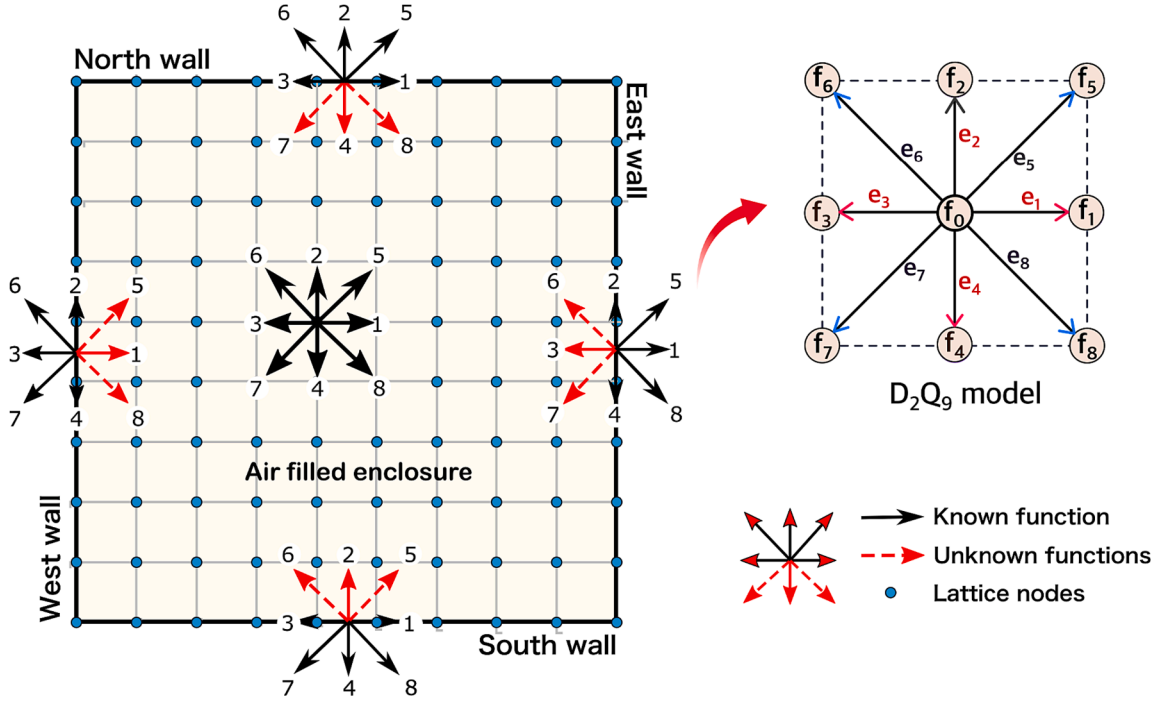


**Fig. 2.** Lattice structure, boundary treatment and velocity vector of the $D_2Q_9$ model [23,25].

$$\rho = \sum_{i=0}^{8} f_i \tag{13}$$

and

$$\rho V = \sum_{i=1}^{8} e_i f_i + \frac{\Delta t}{2}\rho F \tag{14}$$

The fluid's actual velocity ($U$) through the permeable region is determined as follows:

$$U = \frac{V}{c_0 + \sqrt{c_0^2 + c_1|V|}} \tag{15}$$

In this equation, the calculation of '$c_0$' and $c_1$ are done by the following equation:

$$c_0 = \frac{1}{2}\left(1 + \epsilon\frac{\Delta t}{2}\frac{v}{K}\right); c_1 = \epsilon\frac{\Delta t}{2}\frac{c_F}{\sqrt{K}} \tag{16}$$

The additional force term $F_b$ in Eq. (7) refers to buoyancy force responsible for free convection. $F_b$ is computed using the Boussinesq approximation, as expressed in the following equation [24]:

$$F_b = 3w_i g\beta\theta e_{iy} \tag{17}$$

Here, $e_{iy}$ denotes the velocity vector in the direction of gravity.

*Equation for thermal field*

The values of temperature are determined from the"$g$" distribution function using the following equation:

$$g_i(x + e_i\Delta t, t + \Delta t) - g_i(x,t) = -\frac{1}{\tau'}[g_i(x,t) - g_i^{eq}(x,t)] \tag{18}$$

The thermal relaxation time ($\tau'$) is calculated with Chapman-Enskog Equation written as follows:

$$\alpha = (\tau' - \frac{1}{2})\Delta t c_s^2 \tag{19}$$

The equilibrium distribution function, denoted by $g_i^{eq}$, is determined with the following equation:

$$g_i^{eq} = w_i\theta[1 + 3(e_i \cdot U)] \tag{20}$$

The fluid's temperature ($\theta$) is determined by the summation of the "g" distribution function.

$$\theta = \sum_{i=0}^{8} g_i \tag{21}$$

*Boundary conditions*

The implementation of boundary conditions is a critical aspect of the analysis. The velocity at the walls of the enclosure is specified as $U = 0$, adhering to a no-slip condition. The walls are maintained at a cold temperature, denoted as $\theta = 0$. The temperature of the heated porous cylinder region is defined as $\theta = 1$, while the temperature of the cold porous cylinder is specified as $\theta = 0$. In accordance with the Lattice Boltzmann Method, flow and thermal boundary conditions on the walls are specified separately in terms of the particle distribution functions $f$ and $g$, as outlined in Table 1. The flow boundary condition on the permeable cylinders is determined by the Darcy-Forchheimer term, as discussed in Section 2.3.1 and expressed in Eq (11). To implement this, we define a dummy array throughout the domain, with a value of 1 in the permeable zone and 0 in the fluid region. This array is activated in the porous region, which has a circular shape defined by the following mathematical expression:

$$\sqrt{(x - x_{cen})^2 + (y - y_{cen})^2} \le radii \tag{22}$$

Besides, thermal boundary conditions are applied throughout the entire porous region, not solely on the surface. Within the heated permeable cylinder zone, the value $\theta = 1$ is defined, whereas $\theta = 0$ is set for the cold porous cylinder region. Initially, the fluid inside the enclosure is cold, and thus $\theta = 0$ is specified in the region containing clear fluid. The implementation is further carried out using the equation mentioned below.

$$g_i = \theta^*(w_i + \underline{w_i}) - \underline{g_i} \tag{23}$$

In the above equation, '$i$' denotes the lattice location, $w_i$ specifies the value of weighing factor at the lattice, and the corresponding opposite link is represented by $\underline{w_i}$. The distribution function is denoted as $g_i$ and $\underline{g_i}$ refers to the distribution function for corresponding lattice as well as its opposite lattice link.

**Table 1**
Boundary condition applied to the enclosure's walls when LBM is implemented.

| Wall | Wall boundary conditions | Thermal boundary conditions |
|---|---|---|
| Left | $f_1 = f_3, f_5 = f_7, f_8 = f_6$ | $g_1 = -g_3, g_5 = -g_7, g_8 = -g_6$ |
| Right | $f_3 = f_1, f_7 = f_5, f_6 = f_8$ | $g_3 = -g_1, g_7 = -g_5, g_6 = -g_8$ |
| Top | $f_4 = f_2, f_8 = f_6, f_7 = f_5$ | $g_4 = -g_2, g_8 = -g_6, g_7 = -g_5$ |
| Bottom | $f_2 = f_4, f_6 = f_8, f_5 = f_7$ | $g_2 = -g_4, g_6 = -g_8, g_5 = -g_7$ |

*Dimensionless Parameters*

The governing parameters for the present analysis are dimensionless numbers known as Darcy and Rayleigh numbers. The forces responsible for buoyancy-driven flow are defined based on the Rayleigh number, specified as the Grashoff number ($Gr$) multiplied by the Prandtl number. The Grashoff number represents the ratio of buoyant and viscous forces, while the Prandtl number is the ratio of momentum diffusivity to thermal diffusivity. The Rayleigh number is calculated using the following equation:

$$Ra = \frac{g\beta\Delta TL^3}{\nu\alpha} \tag{24}$$

The Darcy number ($Da$) defines the relative effect of permeability over the cross-sectional area of porous media. It is given by:

$$Da = \frac{K}{D^2} = \frac{K}{N^2} \tag{25}$$

Here, $K$ represents permeability, $D$ refers to the diameter of the porous cylinder, and $N$ denotes the number of lattices within the porous region. Furthermore, the calculation of the Darcy number based on porosity ($\epsilon$) using the Carman-Kozeny relation [26–28] is expressed as:

$$Da = \frac{K}{D^2} = \frac{K}{N^2} = \frac{1}{180}\frac{\epsilon^3 d_p^2}{D^2(1-\epsilon)^2} \tag{26}$$

## Methodology of numerical analysis

The current analysis employs the Lattice Boltzmann Method, a mesoscopic approach. Simulations are conducted using a FORTRAN language based code. Flow and thermal analysis involve the implementation of boundary conditions as described in Section 2.3. Initially, the entire domain has zero velocity. The forces arising from the porous region and buoyant forces are incorporated into the collision equation in terms of $F_i$ and $F_b$. The computation of $F_b$ relies on the Boussinesq approximation, with the Rayleigh number being a governing parameter involving the acceleration due to gravity ($g$). To ensure solution stability, the value of $\sqrt{g\beta\Delta TL}$ must be maintained at or below 0.1 [24].

Convergence is monitored using the following criteria for terminating the calculations:

$$\frac{\sqrt{\Sigma_{ij}[u(i,j)^{n+1}-u(i,j)^{n}]^2}}{\sqrt{\Sigma_{ij}[u(i,j)^{n+1}]^2}} \le 1\times10^{-5}, \frac{\sqrt{\Sigma_{ij}[v(i,j)^{n+1}-v(i,j)^{n}]^2}}{\sqrt{\Sigma_{ij}[v(i,j)^{n+1}]^2}} \le 1\times10^{-5}$$
$$\& \frac{\sqrt{\Sigma_{ij}[\theta(i,j)^{n+1}-\theta(i,j)^{n}]^2}}{\sqrt{\Sigma_{ij}[\theta(i,j)^{n+1}]^2}} \le 1\times10^{-6} \quad (27)$$

In the preceding equation, $i$ and $j$ represent the positions on the computational grid. The variables $u$ and $v$ represent the velocity in the $x$ and $y$ directions, respectively. $\theta$ represents the temperature, and $n$ indicates the number of time steps.

### *Code validation*

The reliability of the present code is confirmed when the results align with those reported in the literature. In this study, the solutions obtained for parameters previously considered by Nithiarasu et al. [19] and Yoon et al. [3] exhibit good agreement with the literature. Besides, the code is adapted to accommodate boundary conditions and parameters defined in Yoon et al. [3], which involve two heated cylinders within a cooled enclosure. Simulations are conducted for cylinder radii ranging from 0.1L to 0.4L and Rayleigh numbers from $10^3$ to $10^5$. The code is further validated against the porous-filled enclosure case presented by Nithiarasu et al. [19] with $Da = 10^{-2}$. The results closely match those reported in the literature, with a percentage error of within 1 %. Detailed results and plots can be found in Fig. 3.

### *Grid dependence tests*

The present study involves various cylinder arrangements within the enclosure, including vertical, horizontal, and diagonal orientations. To ensure grid-independent results, the analysis assesses whether the solution remains consistent beyond a certain mesh size. It is crucial to accurately capture the flow and heat transfer phenomena near the porous region and walls. A uniform mesh with a lattice size of one is employed. Mesh sizes of 100 × 100, 200 × 200, 300 × 300, 400 × 400, 500 × 500, and 600 × 600 are tested for all orientations. The results obtained for intermediate parameters, specifically a Rayleigh number of $10^5$ and a Darcy number of 10 nusselt, are presented in Fig. 4. As depicted in the figure, it is evident that the solution remains relatively unchanged beyond a grid size of 500 × 500. To strike a balance between reliable results and computational efficiency, the simulations are subsequently performed using this mesh size.

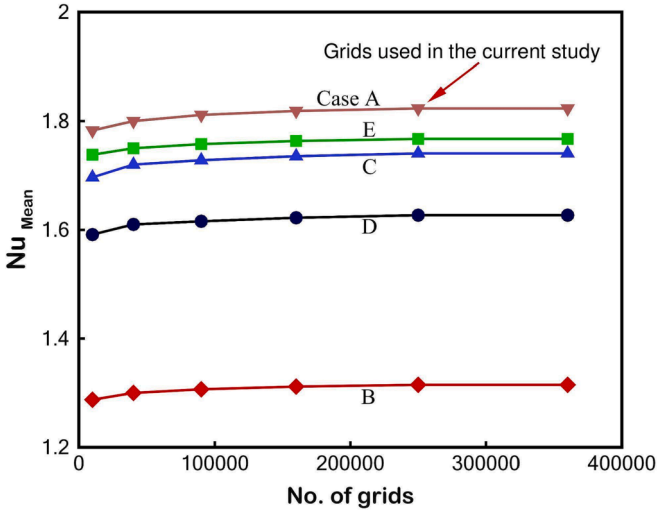


**Fig. 4.** Grid independence analysis for various cylinder arrangements considered in this study.

## Results and discussion

The numerical analysis of free convection within an enclosure containing differentially heated porous cylinders is conducted. The study examines the impact of cylinder placement in vertical, horizontal, and diagonal orientations on the overall thermal performance of the enclosure.

Various dimensionless parameters are considered:

- Darcy number ($Da$): $10^{-6}$, $10^{-4}$, and $10^{-2}$
- Porosity (∈): 0.629, 0.977, and 0.993. These values correspond to $Da = 10^{-6}$, $10^{-4}$, and $10^{-2}$, respectively, as calculated according to Eq. (26).
- Rayleigh Number ($Ra$): $10^4$, $10^5$, and $10^6$

In order to capture a diverse and representative spectrum of natural convection heat transfer, we chose the Rayleigh number range between $10^4$ and $10^6$. We chose this range as it encompasses conditions ranging from moderate to strong buoyancy effects, enabling a comprehensive exploration of convective heat transfer behaviours. At the lower end of the spectrum ($Ra = 10^4$), the Rayleigh number represents scenarios where buoyancy forces are relatively low, allowing for an examination of transitional states. As the Rayleigh number extends towards $10^6$, the investigation includes situations where buoyancy-driven effects become

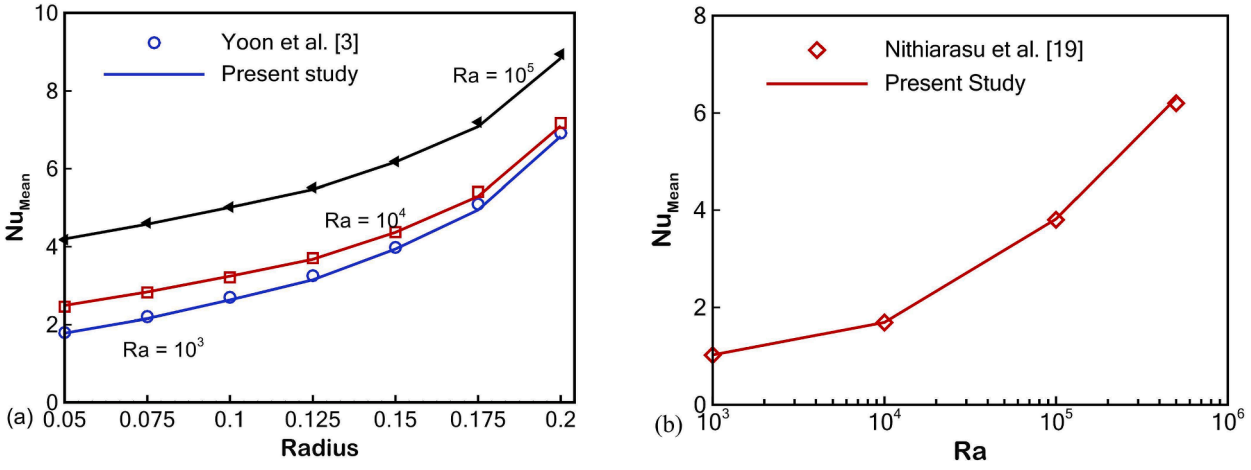


**Fig. 3.** Comparison of computed mean Nusselt number with the literature.

increasingly dominant, leading to intensified convective flows and intricate thermal patterns. By incorporating this broad Rayleigh number range, we aim to provide a detailed understanding of natural convection dynamics across a spectrum of real-world applications, facilitating insights that can inform engineering practices and design considerations.

Also, fluid flow remains in a steady regime within the range of Rayleigh numbers $10^4$-$10^6$, transitioning to an unsteady state at $Ra = 10^7$ [4]. The primary objective of the current study is to investigate enhancing heat transfer through the natural convection mode in a steady flow regime. Therefore, the Rayleigh number range of $10^4$–$10^6$ has been considered in this analysis. Several other works have also employed this range of *Ra* [3–10].

In the subsequent sections we provide a detailed discussion of the numerical investigation outcomes. Local Nusselt number (*Nu*) plots depict the Nusselt number across the enclosure walls, including the top, bottom, and side walls, as well as the entire enclosure walls. The Enhancement Ratio (ER) table illustrates the increase in Nusselt number concerning the lower Darcy number ($10^{-6}$). Streamlines and isotherms are employed to visualize the flow and thermal fields within the enclosure.

### *Local Nusselt number*

The rate of heat transfer at any point on the wall is determined by the local Nusselt number, which measures the ratio of convective to conductive heat transfer. The local Nusselt number is defined as:

$$Nu_l = -\frac{\partial \theta}{\partial n} \tag{32}$$

In Fig. 5, the profile of the local Nusselt number for the cold enclosure walls is presented for Rayleigh numbers ranging from $10^4$ to $10^6$. It is observed that the peak value occurs at the midpoint of the top wall, while the lowest value, nearly zero, is observed at the corners of the enclosure. This pattern is consistent regardless of the Rayleigh number, Darcy number, or the arrangement of differentially heated cylinders. These findings indicate that maximum heat transfer occurs from the top wall.

In Fig. 5(a) and 5(b) at $Ra = 10^5$, the maximum value is observed in the case of diagonal arrangement when the upper cylinder is heated. When $Da = 10^{-6}$, in Case A, two local maxima are seen near the midpoint of the top wall. This is due to the upper hot cylinder's proximity to the cold wall, resulting in maximum heat transfer from the top wall to the outside. In Cases A, C, and E, the local Nusselt number at the bottom wall is almost zero, indicating negligible heat transfer. This is because the heated, less dense fluid rises to the upper section of the enclosure, primarily transferring heat from the top wall. As the Darcy value increases, the magnitude of the peak value also increases, as a larger volume of cold fluid exchanges heat by passing through the hot cylinder. The Nusselt number profile of Case C, the horizontal arrangement, exhibits local maxima at the midpoints of the top and bottom walls. Since the hot and cold cylinders are equidistant from the vertical center, maximum heat exchange occurs along the centerline, followed by heat transfer from the midpoints of the top and bottom walls.

The multiple peaks in Fig. 5(a) diminish at $Da = 10^{-2}$, and the local Nusselt number in proximity to the bottom wall drops to zero for all cylinder arrangements. In addition, local maxima are observed in the upper sections of the left and right walls as the lighter hot fluid rises in the top section of the enclosure. However, the peak value significantly increases as a larger amount of fluid passes through the hot cylinders, leading to an enhanced rate of heat transfer from the top wall. In

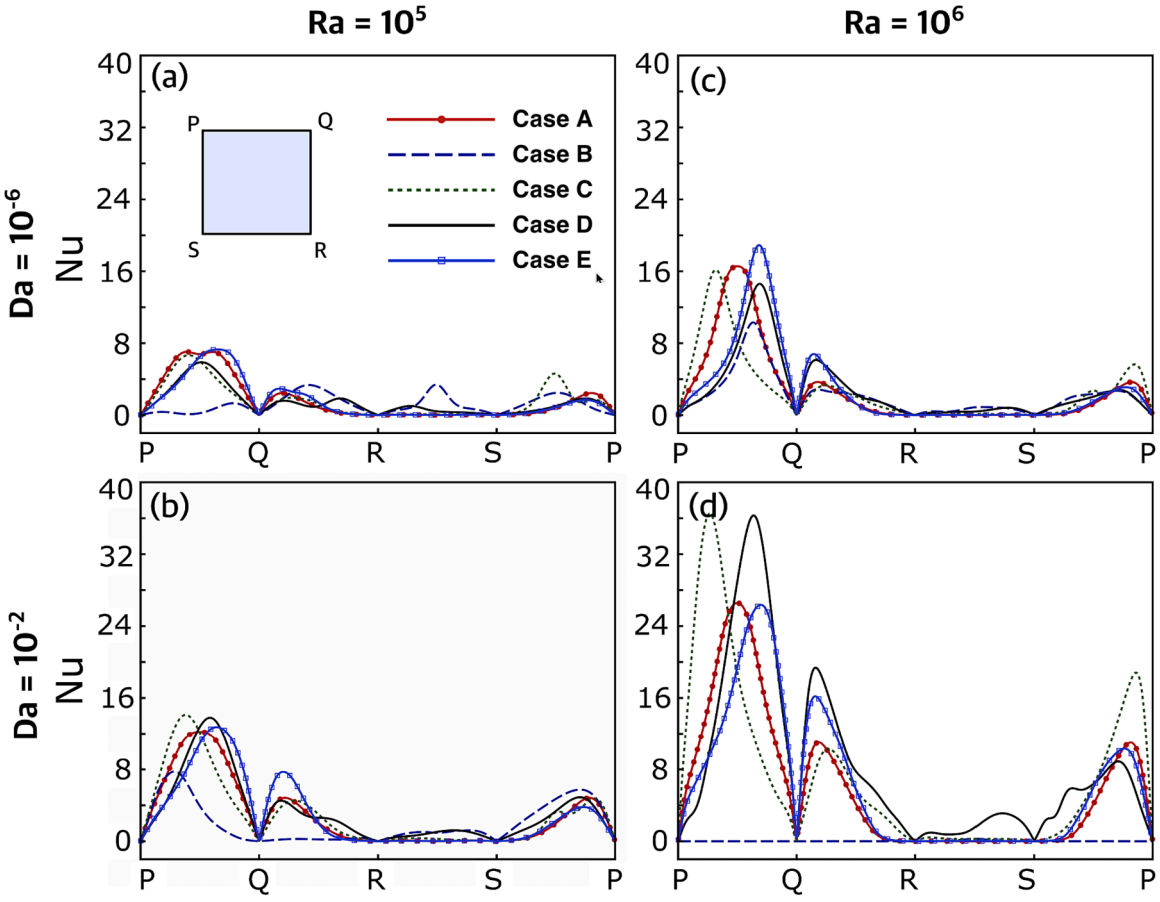


**Fig. 5.** Variations of the local Nusselt number along enclosure walls for different cylinder arrangements at various Rayleigh numbers: (*a, c*) $Da = 10^{-6}$ and (*b, d*) $Da = 10^{-2}$.

summary, the majority of heat dissipates through the upper section walls, while the lower section of the enclosure exhibits minimal heat transfer.

Furthermore, at $Ra = 10^6$, a remarkable enhancement in the *Nu* peak value is observed, illustrating the influence of stronger buoyant forces. When $Da = 10^{-6}$ (as shown in Fig. 5(c)), the maximum value is achieved in Case E when the upper diagonal cylinder is heated. The local Nusselt number increases steadily as we move towards the center of the upper wall and then decreases along the wall ends. The peaks on the side walls are more pronounced compared to those in Fig. 5(a). The reduced distance between the hot cylinder and the side wall in the diagonal arrangement intensifies the *Nu* value, as the combined effects of convection and conduction contribute to heat transfer. A slight increase in the local maxima of the side walls is observed for the vertical arrangement (Cases A and B). Conversely, a decrease in the maximum peak value is observed for the bottom wall in Case B in Fig. 5(c) compared to Fig. 5(a). This is due to larger Rayleigh values inducing stronger buoyant forces, resulting in reduced heat transfer from the bottom wall and an enhancement in heat transfer through the top and side walls of the enclosure. Moreover, with an increase in permeability to $Da = 10^{-2}$, the peak value is obtained for the horizontal arrangement (Case C) in Fig. 5 (d). The fluid passing through the hot cylinder comes into contact with fluid from the cold cylinder, further rises upwards, and hence, the peak is obtained on the section of the wall just above the heated cylinder.

In Case A, the hot cylinder is positioned very close to the top wall, resulting in stronger thermal plumes pointing at the midpoint. As a consequence, the *Nu* profile along the top wall is symmetric. In Case B, the heated fluid from the lower cylinder rises upwards, exchanging heat with the upper cylinder and cooling down. Simultaneously, the heavier cold fluid flows downward towards the hot cylinder, causing recirculation within the enclosure. Consequently, minimal heat transfer occurs from the enclosure walls, a fact confirmed by the nearly zero *Nu* values for all four enclosure walls.

In Case D, multiple peaks are observed on the enclosure walls close to the heated cylinders. The temperature difference between the hot cylinder and the enclosure walls serves as a driving force, resulting in peaks in the *Nu* profiles along the sections of enclosure walls in proximity to the hot cylinder. In this case, the profile of the bottom wall rises until a section near a hot cylinder and then drops suddenly. In contrast, in the other cases, the local Nusselt number for the bottom wall is negligible. Therefore, heat transfer from the bottom wall occurs in the case of the diagonal arrangement when the hot cylinder is near the bottom wall. Since local peaks are observed along all four walls of the enclosure in Case D, it can be inferred that the overall heat transfer in this case is the highest among all cases.

### *Mean Nusselt number*

The calculation of mean Nusselt number is done according to the following formula:

$$Nu_{Mean} = \frac{1}{L}\int_0^L Nu_l dL \tag{33}$$

### *Mean Nusselt number of walls*

Fig. 6 displays the mean Nusselt numbers for the top ($Nu_T$), bottom ($Nu_B$), and sidewalls ($Nu_S$) over a range of *Ra* ($10^4$ —$10^6$) and Da ($10^{-6}$ – $10^{-2}$). Various arrangements of differentially heated cylinders impact the heat transfer from the walls, with the average Nusselt numbers for the top wall generally being higher in most cases.

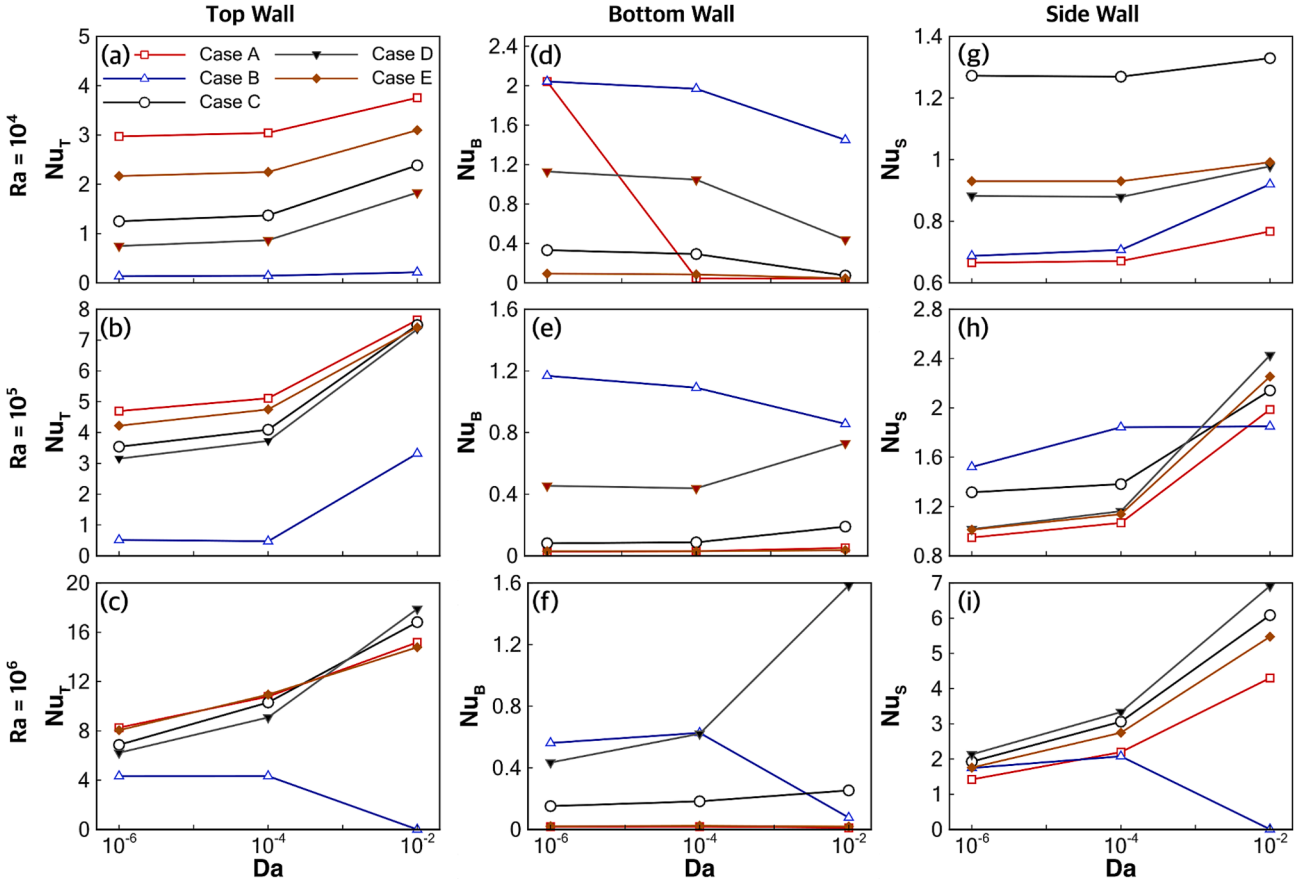


**Fig. 6.** Variations of the mean Nusselt Number along the enclosure walls for various cylinder arrangements with Darcy numbers of $10^{-6}$, $10^{-4}$, and $10^{-2}$, presented separately for (*a*)-(*c*) the top wall, (*d*)-(*f*) the bottom wall, and (*g*)-(*i*) the side wall.

For $Ra = 10^4$ and $10^5$, in Case A (top hot, bottom cold), the upward flow of air through the hot cylinder results in maximum heat transfer from the top wall, as shown in Figures (a) and (b). Interestingly, in Figure (c) at Ra = $10^6$ and $Da = 10^{-2}$, the highest $Nu_T$ value is observed for Case D, where the left upper cylinder is heated, and the right lower cylinder is cold in a diagonal arrangement. Conversely, Case B consistently exhibits the lowest $Nu_T$ value, regardless of parameter variations. This is because in Case B, as the hot fluid rises, exchanges heat with the upper cold cylinder, and then flows toward the lower section of the confinement, it gets cooled before reaching the top wall. Moreover, cold fluids stagnate near the top wall and upper cold cylinder, resulting in minimal heat transfer from the top wall with this cylinder arrangement.

In Figures (d) to (f), it is evident that an increase in Rayleigh number leads to a decrease in the average Nusselt number of the bottom wall ($Nu_B$). At $Ra = 10^4$, an increase in Darcy number reduces the $Nu_B$ value. Case B has the highest $Nu_B$ value among all cases due to the proximity of a hot cylinder to the bottom wall, followed by a continuous drop in value with increases in Rayleigh and Darcy numbers. Maximum heat transfer occurs from the bottom wall in this case. At Rayleigh value $10^5$, the increase in Darcy value has minimal effect on $Nu_B$ for all cases considered. However, with further increases in Ra to $10^6$, the $Nu_B$ value significantly increases from $Da = 10^{-4}$ to $10^{-2}$ in Case D. This is attributed to an increased volume of fluid passing through the hot cylinder placed at the bottom-right corner and the presence of stronger convective forces, which intensify heat transfer from the bottom wall. The $Nu_B$ values for cases A and E remain minimal and unaffected by changes in Rayleigh and Darcy numbers, as the heated cylinders in these arrangements are close to the top wall, resulting in minimal heat transfer from the bottom wall.

The average Nusselt number of the sidewalls ($Nu_S$) continuously increases with increasing Rayleigh and Darcy numbers for cases A, C, D, and E (Figures (g) to (i)). At $Ra = 10^4$, Case B with a horizontal arrangement exhibits the maximum $Nu_S$ value for all Darcy numbers. In this arrangement, cylinders are placed along the horizontal centerline of the enclosure, and conduction effects are stronger, leading to higher heat transfer from the walls near the cylinders. At Rayleigh number $10^6$, the maximum $Nu_S$ value is obtained in Case D. The right wall is close to a hot cylinder placed near the bottom-right corner, resulting in heat transfer through the region near the right wall. The intensified buoyant effects divert the flow direction towards the cold cylinder, placed near the left wall. Consequently, a significant amount of heat exchange occurs in regions in close proximity to the left wall. Therefore, the sidewalls transfer more heat in the case of this diagonal arrangement of cylinders.

*Mean Nusselt number of enclosure*

The mean Nusselt numbers for the enclosures are illustrated in Fig. 7. Figs. 9–12 (d)-(f) shows the streamlines and thermal contours when the upper cylinder is cold and lower is heated (case B). At $Ra = 10^4$, two secondary vortices generated above the cold cylinder. This is in contrast to the previous case. The hot fluid from the heated lower cylinder is lighter and flows towards the cold cylinder. The induced buoyancy forces due to cold cylinder exchanges heat and temperature of recirculating fluid drops. In this case, the overall thermal performance of the system is less as heated fluid continuously cools down as the cold cylinder is placed upwards. On increasing the Rayleigh number to $10^6$, the distorted symmetry is seen for $Da = 10^{-6}$ and $10^{-4}$ and it is regained at $Da = 10^{-2}$. The primary vortices are oriented in the direction of the bottom wall and secondary vortices are formed near corners of the enclosure. When Darcy number enhances, the fluid interacts with increased surface

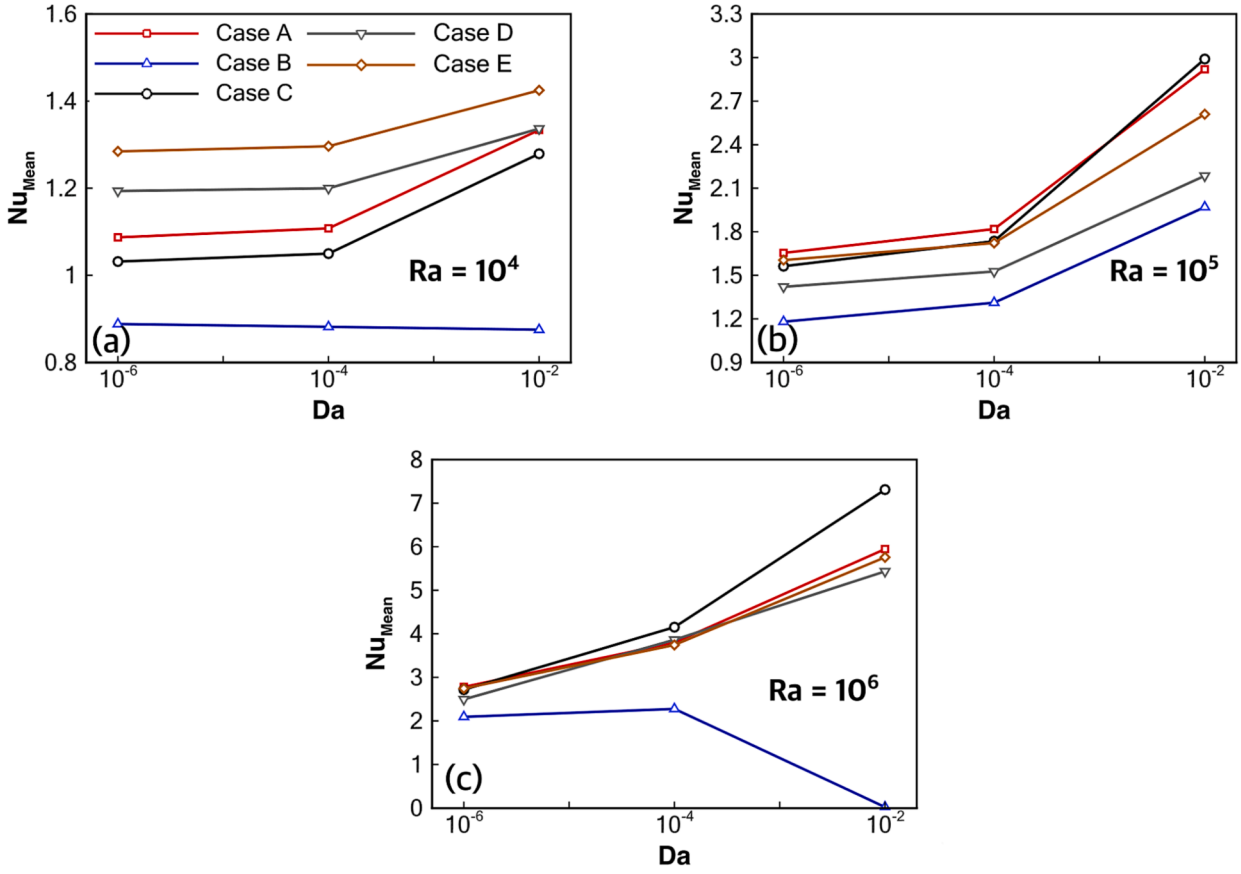


**Fig. 7.** Variations in the mean Nusselt Number of the enclosure for different cylinder arrangements at (a) $Ra = 10^4$, (b) $Ra = 10^5$, and (c) $Ra = 10^6$, with Da values of $10^{-6}$, $10^{-4}$ and $10^{-2}$.

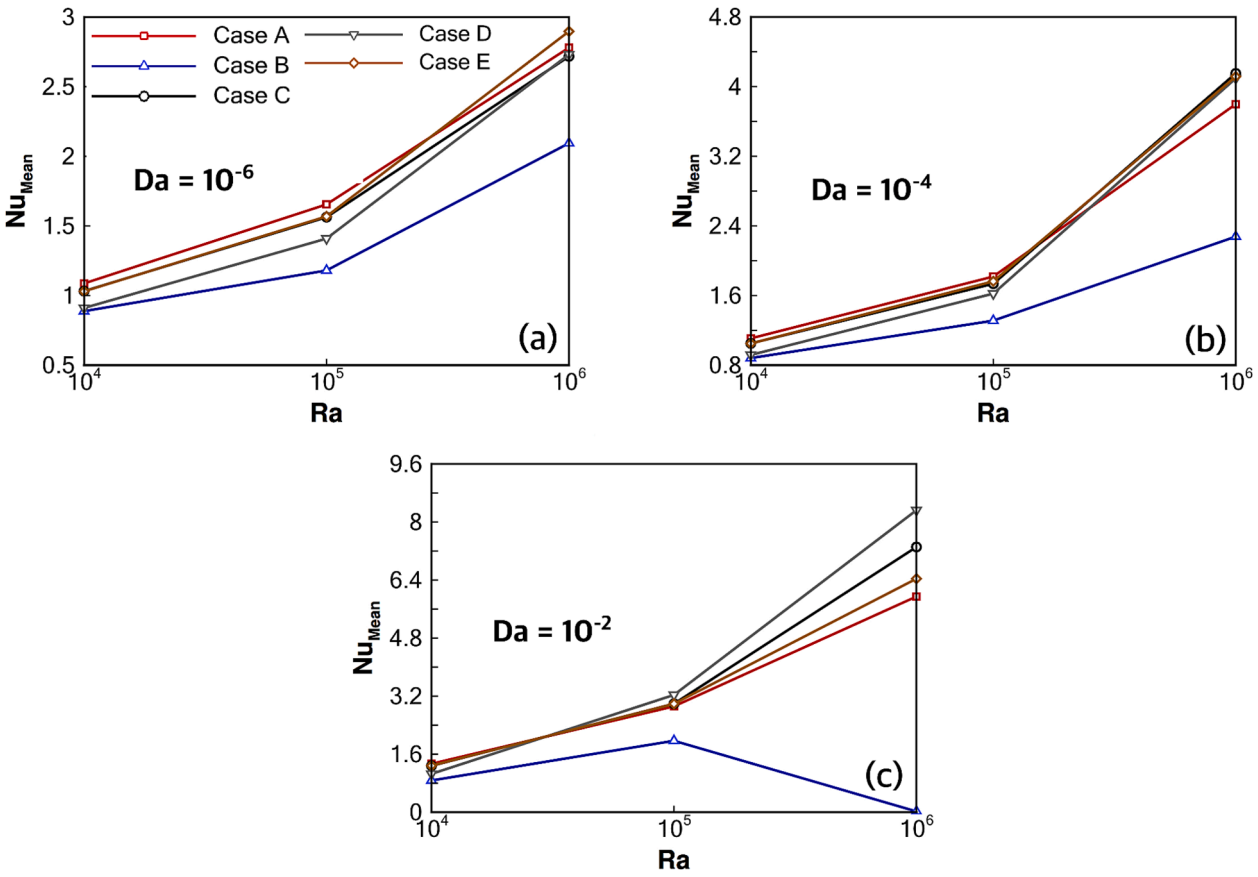


**Fig. 8.** Variations in the mean Nusselt Number of the enclosure for different cylinder arrangements at (a) $Da = 10^{-6}$, (b) $Da = 10^{-4}$, and (c) $Da = 10^{-2}$, with $Ra$ values of $10^4$, $10^5$ and $10^6$.

area due to high permeable region and hence enhanced heat transfer occurs. The enclosure's overall heat transfer rate is minimum in this case as compared to all other cases as cooling of fluid occurs within the enclosure.

The horizontal, vertical, and diagonal orientations of cylinders, the case with a vertical orientation of the upper heated and lower cold cylinder (Case A) exhibits the highest mean Nusselt number for the enclosure at a lower Rayleigh number of $10^4$ (see Fig. 7(a)). In this scenario, heat is primarily transferred through conduction, as viscous forces are relatively stronger. The upper heated porous cylinder is positioned close to the top wall, allowing for the maximum transfer of heat.

Both the horizontal arrangement (Case C) and the diagonal arrangement with the lower cylinder being hot and the upper one being cold (Case E) show an equivalent rate of heat transfer. However, in the case of the lower heated and upper cold cylinder (Case B), the heat dissipates within the enclosure, resulting in minimal heat transfer from the enclosure walls.

At $Ra = 10^5$ (Fig. 7(b)), the buoyant force surpasses viscous forces, leading to heat transfer occurring primarily through convection. In this scenario, Case C, featuring a horizontal arrangement of cylinders with the left one being cold and the right one being hot, attains the highest value at $Da = 10^{-2}$ (Fig. 7(c)).

Fig. 8 (a)-(c) depicts the influence of Rayleigh number on mean Nusselt number of enclosures for various Darcy values ranging from $10^{-6}$ to $10^{-2}$. The convection rate enhances with Rayleigh numbers. The conductive forces are dominant at $Ra = 10^4$, hence, heat flows with low velocity from hot cylinder towards enclosure. Therefore, smaller values of the mean Nusselt number can be seen irrespective of Darcy number. By increasing the Rayleigh value to $10^5$, the buoyant forces are enhanced, resulting in the initiation of convection effects. Consequently, a greater amount of fluid enters the cylinders and circulates, transferring heat from the heated cylinder to the cooled enclosure wall due to temperature gradient. When the Rayleigh number rises to $10^6$, convective effects become stronger as the fluid velocity enhances. This results in larger amounts of fluid entering the porous cylinders. Henceforth, significant augmentation in heat transfer rates are obtained.

It can also be deduced from Fig. 8 (a)-(c) that an increment in $Ra$ value results in heat transfer enhancement along with Darcy number. The influence of permeability can be analyzed with Darcy numbers. In Fig. 8 (a), when $Da = 10^{-6}$, minimal variation is seen with increasing Rayleigh values. The greater viscous resistance allows for the little volumes of fluid to enter the cylinder. Hence, lower values of mean Nusselt number are obtained indicating less heat transfer. In addition, varying arrangement of cylinders has insignificant impact on mean Nusselt number value. As the Darcy number increases to $10^{-4}$, it can be seen from (Fig. 8 (b)) that the magnitude of Nusselt number increases. The variation in permeability allows the fluid to enter cylinders and enhance heat transfer rates.

Further, at $Da = 10^{-2}$ (Fig. 8 (c)), the mean Nusselt number intensifies, as the fluid flows with more ease through cylinders carrying larger amounts of heat. Thus, thermal transfer rates escalate. However, in case B, $Nu$ drops to near zero when $Ra = 10^6$. The heated lower cylinder emits a hot fluid that is less dense and moves towards the colder cylinder. The cold cylinder generates stronger buoyancy forces that cause a decrease in the heat and temperature of the recirculating fluid. In this scenario, the system's thermal performance is reduced because the heated fluid consistently loses heat when the cold cylinder is positioned over it.

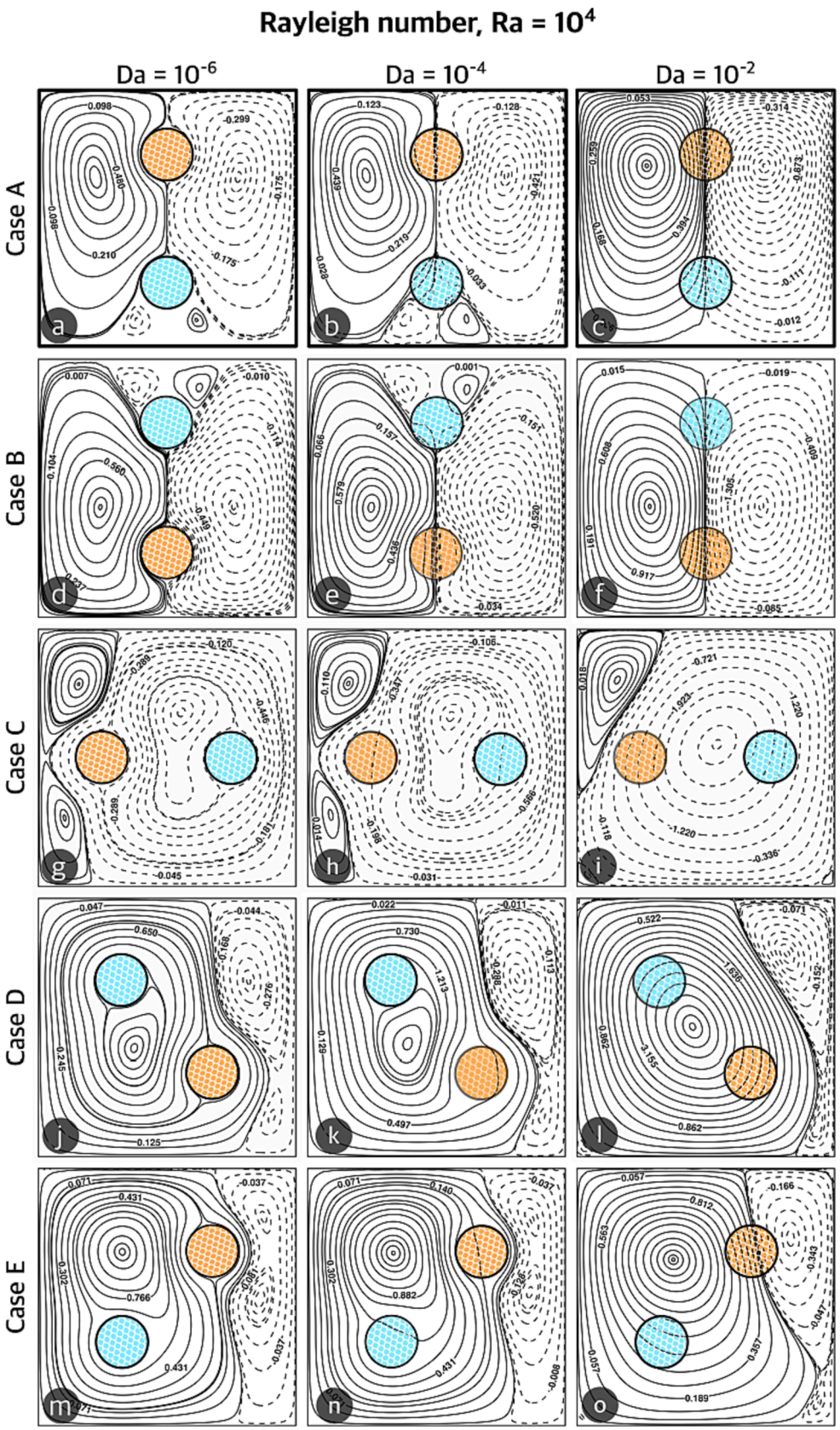


**Fig. 9.** Streamlines in and around the porous cylinders for Rayleigh number, $Ra = 10^4$ and Darcy numbers, $Da = 10^{-6}$, $10^{-4}$ and $10^{-2}$.

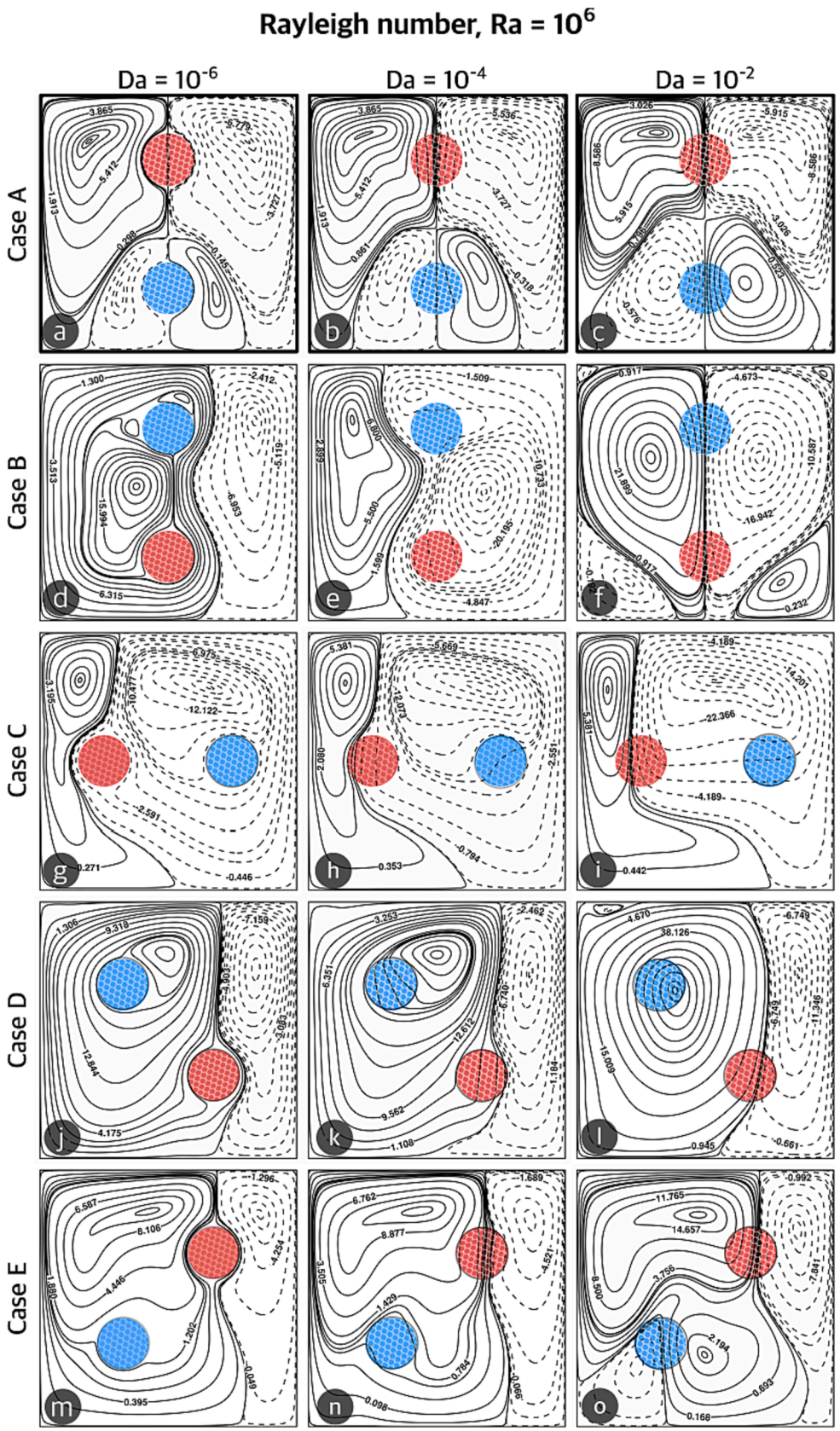


**Fig. 10.** Streamlines in and around the porous cylinders for Rayleigh number, $Ra = 10^6$ and Darcy numbers, $Da = 10^{-6}$, $10^{-4}$ and $10^{-2}$.

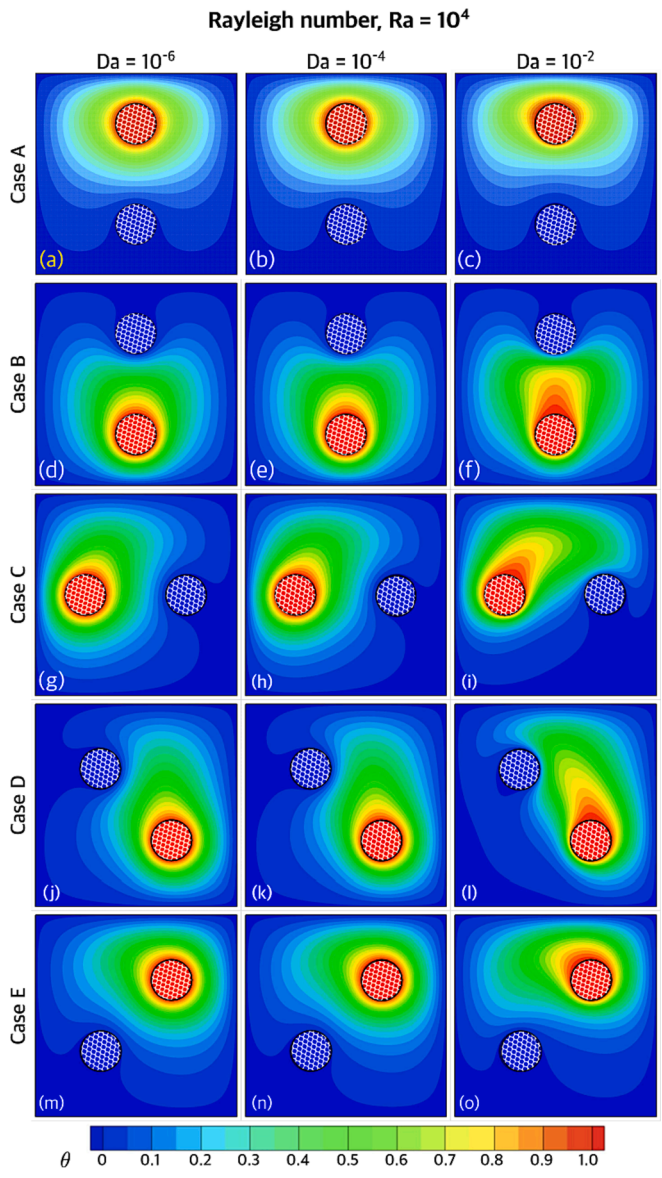


**Fig. 11.** Isotherms around the porous cylinders are shown for different Darcy numbers ($10^{-6}$, $10^{-4}$, and $10^{-2}$) at a Rayleigh number of $Ra = 10^4$. The mesh-like structures inside the hot and cold cylinders are included for representation purposes only to illustrate the porous nature of the cylinders. Otherwise, the hot cylinder is filled with red colour, and the cold cylinder is filled with blue colour. (For interpretation of the references to colour in this figure legend, the reader is referred to the web version of this article.)

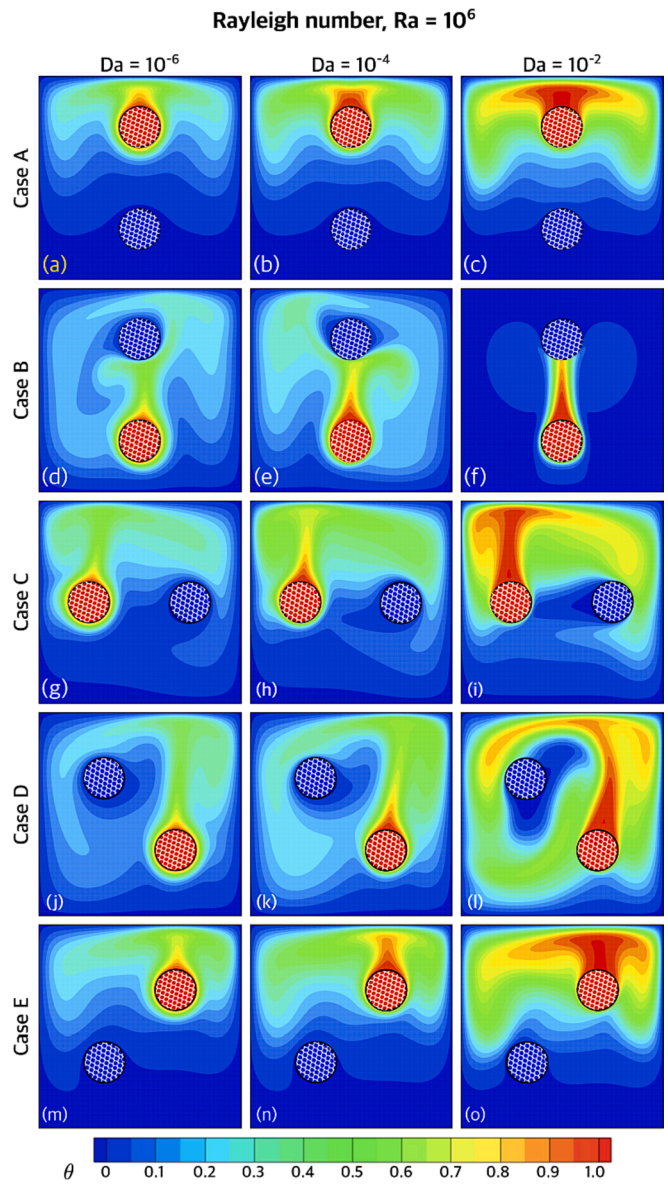


**Fig. 12.** Isotherms around the porous cylinders are shown for different Darcy numbers ($10^{-6}$, $10^{-4}$, and $10^{-2}$) at a Rayleigh number of $Ra = 10^6$. The mesh-like structures inside the hot and cold cylinders are included for representation purposes only to illustrate the porous nature of the cylinders. Otherwise, the hot cylinder is filled with red colour, and the cold cylinder is filled with blue colour. (For interpretation of the references to colour in this figure legend, the reader is referred to the web version of this article.)

*Enhancement ratio*

To compare the heat transfer enhancement of a porous cylinder with that of a solid cylinder (in the $Da = 10^{-6}$ case), we calculated the heat transfer enhancement ratio (ER), defined as the ratio of the Nusselt number ($Nu$) of the enclosure to the Nusselt number of the enclosure at $Da = 10^{-6}$. It is expressed as:

$$ER = \frac{Nu}{Nu_{Da=10^{-6}}} \tag{34}$$

Table 2 shows the Enhancement Ratio at $Da = 10^{-4}$ and $Da = 10^{-2}$. This data allows us to analyze the overall enhancement in heat transfer for different configurations. When $Ra = 10^4$, the enhancement is relatively low, with the highest ER value for $Da = 10^{-4}$ attained in Case A being 1.019. The hot cylinder is close to the upper wall, and heat flows directly towards the top wall due to stronger conductive forces. Furthermore, at $Da = 10^{-2}$, the maximum value achieved for Case C is 1.239, and for Case E, it is 1.244. In this scenario of Case C, the cylinders are positioned along the horizontal centerline of the enclosure. The stronger viscous forces drive heat toward the walls, resulting in maximum heat transfer compared to other configurations.

However, when the Rayleigh value is increased to $10^5$ and $10^6$, a sudden increment in ER is observed. The substantial impact of buoyant forces intensifies the enhancement in heat transfer, with the maximum ER value at $Da = 10^{-2}$ and $Ra = 10^5$ being 2.294, and at $Ra = 10^6$ being 3.048, obtained in Case D. In this scenario, the cylinders are diagonally aligned, with the heated cylinder located at the bottom corner. The lighter-density hot fluid directs itself towards the region near the cold cylinder, facilitating heat transfer to the outside through all walls of the enclosure.

As the results indicate, for all $Ra$ and $Da$ values considered, the

**Table 2**
Heat transfer enhancement ratio (ER) for different arrangement of cylinders at $Ra = 10^4$, $10^5$ and $10^6$, and $Da = 10^{-4}$ and $10^{-2}$.

| | Ra = $10^4$ | |
|---|---|---|
| Case | $Da = 10^{-4}$ | $Da = 10^{-2}$ |
| A | 1.019 | 1.227 |
| B | 0.993 | 0.986 |
| C | 1.018 | 1.239 |
| D | 1.008 | 1.160 |
| E | 1.018 | 1.244 |
| | Ra = $10^5$ | |
| Case | $Da = 10^{-4}$ | $Da = 10^{-2}$ |
| A | 1.099 | 1.764 |
| B | 1.111 | 1.670 |
| C | 1.110 | 1.913 |
| D | 1.150 | 2.294 |
| E | 1.124 | 1.905 |
| | Ra = $10^6$ | |
| Case | $Da = 10^{-4}$ | $Da = 10^{-2}$ |
| A | 1.366 | 2.139 |
| B | 1.087 | 0.0104 |
| C | 1.528 | 2.690 |
| D | 1.499 | 3.048 |
| E | 1.420 | 2.221 |

minimum ER value is observed for Case B. The ER value drops to 0.0104 (near zero) for $Ra = 10^6$ and $Da = 10^{-2}$. In this configuration, the fluid from the lower hot cylinder flows upwards, interacts with the cold cylinder, undergoes heat exchange, and then flows in a downward direction. Consequently, heat is not transferred toward the enclosure walls, but rather continuous cooling occurs.

*Streamlines and isotherms*

The overall fluid flow patterns are visualised using streamlines in Figs. 9 and 10, while thermal fields with isotherms are displayed in Figs. 11 and 12. The Rayleigh number, Darcy number, and the orientation (vertical, horizontal, and diagonal) of the hot and cold cylinders exert a significant influence on both the flow and thermal fields. It is important to note that, for all the parameters considered, the fluid flow regime remains in a steady state. The path of air circulation through the porous cylinders within the enclosure varies in response to changes in the magnitude of buoyancy-induced forces and porosity values. Furthermore, the thermal mixing occurring within the enclosure is contingent upon gravitational forces.

*Influence of Rayleigh number*

The Rayleigh number defines the relationship between buoyant and viscous forces, as well as the thermal and momentum diffusion of heat within a fluid. Consequently, it serves as a key indicator of the intensity of natural convective effects. Figs. 9–12 illustrate the impact of the Rayleigh number on flow and thermal patterns. At $Ra$=$10^4$, the streamlines recirculate near the cylinders due to the slow fluid flow. Symmetrical contours emerge along the vertical centerline of the enclosure when cylinders are placed vertically or horizontally. The dominance of viscous forces and thermal diffusivity leads to limited fluid penetration inside the cylinders. Here, an increase in the Darcy number has minimal impact on heat transfer, and the isotherms remain distant and parallel due to the prevalence of conductive effects.

As the Rayleigh number is increased to $10^5$, a combination of conduction and convection for heat transport becomes evident. Buoyancy-induced forces, in conjunction with conductive forces, contribute to heat transfer. Viscous forces weaken, allowing a greater quantity of fluid to enter the cylinders. Consequently, substantial effects of porosity are observed in both streamlines and isotherms.

When $Ra$=$10^6$, buoyancy-induced forces are significantly stronger, and convective effects become dominant. The symmetry of flow and thermal contours distorts as fluid circulates at an intensified velocity (see Fig. 10 and Fig. 12). Primary vortices extend from the hot cylinder to the cold cylinder, subsequently directing towards the enclosure wall in all cylinder configurations. The permeability of the cylinders exerts pronounced effects at higher Rayleigh numbers, as strong inertial forces overpower viscous forces, allowing large volumes of fluid to pass through. Thermal plumes near the cold cylinders become more twisted, and this effect is clearly evident in the isotherms. Besides, a thinner thermal boundary layer forms on the cylinder's surface.

*Influence of differentially heated cylinders orientation*

Two porous cylinders, each at different temperature levels, are positioned in various configurations: vertically, horizontally, and diagonally within an enclosure. The position and orientation of these heated and cold cylinders exert a notable influence on the streamlines and isotherms. The impact of these factors on flow patterns and temperature fields is visually depicted in Figs. 9–12. A more comprehensive discussion is provided in the subsequent section.

*CASE A: Hot upper cylinder and cold lower cylinder.* In this configuration, two porous cylinders of different temperatures are positioned vertically, with the upper cylinder being heated and the lower one cooled. The corresponding figures are displayed in Figs. 9–12 (a)-(c). The flow field exhibits symmetry with respect to the *y*-axis, regardless of variations in Rayleigh and Darcy numbers. Among all the cases studied, this arrangement demonstrates the highest heat transfer from the enclosure, especially at lower Rayleigh numbers ($10^4$), irrespective of Darcy number variations.

Despite relatively poor fluid circulation around the cylinders due to weaker buoyant forces, this arrangement facilitates efficient heat transfer. In this scenario, the elliptical-shaped inner vortices transform into circular patterns as the Darcy number increases to $10^{-2}$. Primary vortices are observed extending from the cylinders towards the walls within the enclosure. Also, the height of secondary vortices between the lower cylinder and the bottom wall decreases as a larger quantity of fluid enters the cylinder.

The heated cylinder emits thermal plumes that rise upwards because the less dense hot fluid in the vicinity of the upper heated cylinder ascends. Notably, heat transport is not significantly influenced by the buoyant forces resulting from temperature differences. The presence of a cold cylinder does not markedly affect the overall thermal performance of the enclosure in this case. However, at $Ra = 10^6$, the region of secondary vortices expands, leading to more circulation of cold fluid near the cold cylinder. When $Da = 10^{-2}$, primary eddies tend to move upwards, and the height of the secondary vortex further increases as a substantial amount of fluid enters both the cold and heated cylinders. The isotherms spread in the region between the upper cylinder and the top wall, indicating maximum heat transfer from this wall. In this case, the presence of a cold cylinder plays a minimal role in heat transfer from the entire confinement.

*CASE B: Cold upper cylinder and hot lower cylinder.* Figs. 9–12 (d)-(f) display streamlines and thermal contours when the upper cylinder is cold and the lower one is heated. At $Ra = 10^4$, two secondary vortices form above the cold cylinder, in contrast to the previous case. The lighter hot fluid from the heated lower cylinder flows towards the cold cylinder, driven by induced buoyancy forces, leading to an exchange of heat and a drop in the temperature of the recirculating fluid. In this scenario, the overall thermal performance of the system is reduced because the heated fluid continuously cools down as the cold cylinder is positioned above.

As we increase the Rayleigh number to $10^6$, we observe distorted symmetry at $Da = 10^{-6}$ and $10^{-4}$, which is restored at $Da = 10^{-2}$. The primary vortices align with the direction of the bottom wall, and

secondary vortices form near the corners of the enclosure. With an increasing Darcy number, the fluid interacts with a larger surface area due to the highly permeable region, leading to enhanced heat transfer. In this case, the enclosure's overall heat transfer rate is at its minimum compared to all other cases because fluid cooling occurs within the enclosure.

*CASE C: Hot left cylinder and right cold cylinder.* In this case, the cylinders are positioned horizontally, with the left cylinder heated and the right cylinder cooled. Heat is transferred from the heated left cylinder to the cold right cylinder. Heat transfer is reduced in the horizontal cylinder orientation compared to the vertical orientation at lower Rayleigh number values. At $Ra = 10^4$, a primary clockwise vortex forms along the left wall due to the proximity of the heated cylinder (as shown in Fig. 9 (g)-(i)). An anti-clockwise recirculating vortex is observed near the cylinders. The hotter fluid rises towards the upper part of the enclosure due to its lower density, but the horizontal cylinder orientation obstructs fluid recirculation towards the lower region. The majority of heat transfer occurs from the top wall, and convection effects are suppressed. Hot fluid accumulates below the heated cylinder and above the cold cylinder, resulting in dense isotherms that incline towards the cold cylinder due to buoyant forces inducing heat flow.

The length of the primary vortex near the bottom wall increases as the Darcy number rises from $10^{-6}$ to $10^{-2}$. Horizontal orientation provides the highest rate of heat transfer for Da values of $10^{-4}$ and $10^{-2}$. Higher Darcy values result in expanded space for recirculation within the enclosure, while smaller recirculating zones are diminished.

The results are similar when the right cylinder is heated, and the left cylinder is cooled. Therefore, this scenario is not further described to avoid redundant explanations and maintain conciseness.

*CASE D: Cold upper-diagonal and hot lower-diagonal.* The diagonal placement of cylinders exhibits the highest rates of heat transfer at higher Rayleigh numbers ($10^5$ and $10^6$). The patterns of streamlines and isotherms undergo significant changes as the cylinders are shifted towards the corners of the enclosure.

When $Ra = 10^4$, primary vortices extend from the lower hot cylinder to the upper cold cylinder. The fluid flows from the hot cylinder towards the cold cylinder, undergoes heat exchange, and then returns to the bottom-right corner of the enclosure. Two secondary vortices form near the corners adjacent to the right wall, impeding heat transfer. In addition, the thermal plumes are closer to the hot cylinder and incline diagonally towards the cold cylinder.

As the Rayleigh number increases to $10^6$, the smallest eddy shifts upward towards the top wall. At $Da = 10^{-2}$, an additional small vortex forms in the corner near the cold cylinder, accompanied by two secondary vortices at the corners along the right wall (as shown in Fig. 10 (j)-(l)). These secondary vortices are suppressed as a higher volume of fluid penetrates inside the cylinders with increasing permeability from $Da = 10^{-6}$ to $10^{-2}$. The intensity of thermal contours strengthens due to enhanced convection effects, as clearly evidenced by the results.".

*CASE E: Hot upper-diagonal and cold lower-diagonal.* When the cylinders are arranged diagonally, with the hot cylinder at the upper side and the lower cylinder being cold, they transfer less heat compared to other configurations. As the hot fluid from the cylinders flows upwards without obstruction, primary vortices span from the heated to the cold cylinder. At $Ra = 10^4$, the size of the clockwise recirculatory region increases as the Darcy value rises from $10^{-6}$ to $10^{-2}$. Further, a small vortex forms near the bottom-right corner. The denser hot fluid with lower velocity expands in the proximity of the hot cylinder placed in the upper region, resulting in a lower heat exchange rate for the cold cylinders.

The average Nusselt number for these enclosures is equivalent to that of the horizontal alignment. However, at $Ra = 10^6$, four small vortices form on the sides of both cylinders (as shown in Fig. 10 (m)-(o)). Anti-clockwise recirculation can be observed in the corners near the cylinders. These vortices indicate stagnation of fluid in the vicinity of the cylinders, resulting in a reduced volume of heated fluid interacting with the cold fluid. In this scenario, the hot fluid recirculates in the upper half section of the enclosure, and as a result, most of the heat transfer occurs from the top wall and the half of the right and left walls. The fluid in proximity to the cold cylinder remains in the lower region, minimizing the transport of heat outside the lower section of the enclosure.

## Conclusions

In this research, the investigation centered on understanding heat transfer dynamics within enclosures housing porous cylinders subjected to differential heating. The analysis of mean Nusselt numbers unveiled intriguing flow patterns and thermal behaviors. At lower Rayleigh numbers ($Ra = 10^4$), the presence of secondary vortices above the cold cylinder, when the upper cylinder was cold and the lower one heated, resulted in buoyancy-driven flow and a drop in fluid temperature. However, this configuration proved to be less thermally efficient. As $Ra$ increased to $10^6$, a brief loss of symmetry was observed for specific Darcy numbers, which was later restored at $Da = 10^{-2}$. Higher Darcy numbers facilitated enhanced heat transfer, albeit with a trade-off of reduced overall heat transfer within the enclosure. The study also explored different cylinder orientations, including horizontal, vertical, and diagonal arrangements, with the vertically oriented heated upper and cold lower cylinder (Case A) emerging as the most efficient for heat transfer at $Ra = 10^4$. At $Ra = 10^5$ and $10^6$, buoyant forces dominated, favouring heat transfer via convection. In these scenarios, the diagonal alignment of cylinders in Case D with the lower cylinder heated proved most effective in maximizing heat transfer through all enclosure walls. Besides, the comparison between porous and solid cylinders at $Da = 10^{-6}$ using the enhancement ratio (ER) highlighted that Case B consistently exhibited the lowest ER value, indicating continuous cooling within the enclosure, while Case C showed the highest ER value at $Ra = 10^4$ due to enhanced viscous forces directing heat toward the walls. This research provides valuable insights for optimizing systems involving porous cylinders within enclosures, taking into account cylinder orientation, buoyancy effects, and heat transfer enhancement considerations.

## CRediT authorship contribution statement

**B. Shruti:** Conceptualiation, Data curation, Writing - Original draft, Writing - review & editing, Visualization, Investigation, Validation, Formal Analysis, Resources, Methodology. **S. Dhinakaran:** Conceptualization, Funding acquisition, Data Curation, Writing - Original Draft, Writing - Original & Editing, Visualization, Investigation, Validation, Formal analysis, Methodology, Supervision, Resources, Project administration and Software.

## Declaration of competing interest

The authors declare the following financial interests/personal relationships which may be considered as potential competing interests: S. Dhinakaran reports financial support and equipment, drugs, or supplies were provided by Indian Institute of Technology Indore.

## Data availability

We affirm that upon request, readers will receive access to the results file. If you need the data, kindly get in touch with the corresponding author.

## References


[1] S. Dhinakaran, J. Ponmozhi, Heat transfers from a permeable square cylinder to a flowing fluid, Energ. Conver. Manage. 52 (5) (2011) 2170–2182, https://doi.org/10.1016/j.enconman.2010.12.027.

[2] S. Bhattacharyya, S. Dhinakaran, A. Khalili, Fluid motion around and through a porous cylinder, Chem. Eng. Sci. 61 (13) (2006) 4451–4461, https://doi.org/10.1016/j.ces.2006.02.012.

[3] H.S. Yoon, J.H. Jung, Y.G. Park, Natural convection in a square enclosure with two horizontal cylinders, Numer. Heat Transf. Part A: Appl. 62 (9) (2012) 701–721, https://doi.org/10.1080/10407782.2012.709438.

[4] F. Moukalled, S. Acharya, Natural convection in the annulus between concentric horizontal circular and square cylinders, J. Thermophys. Heat Transfer 10 (3) (1996) 524–531, https://doi.org/10.2514/3.820.

[5] H.S. Yoon, Y.G. Park, and J. H. Jung (2014) Natural convection in a square enclosure with differentially heated two horizontal cylinders. *Numer. Heat Transfer Part A: Appl.* 65.4 (2014): 302-326. https://doi.org/10.1080/10407782.2013.831679.

[6] B. Shruti, M.M. Alam, A. Parkash, S. Dhinakaran, LBM study of natural convection heat transfer from a porous cylinder in an enclosure, Theor. Comput. Fluid Dyn. (2022), https://doi.org/10.1007/s00162-022-00632-z.

[7] C. J. Ho, W. S. Chang, and C. C. Wang (1993). Natural convection between two horizontal cylinders in an adiabatic circular enclosure : 158-165. https://doi.org/10.1115/1.2910642.

[8] C.J. Ho, Y.T. Cheng, C.C. Wang, Natural convection between two horizontal cylinders inside a circular enclosure subjected to external convection, Int. J. Heat Fluid Flow 15 (4) (1994) 299–306, https://doi.org/10.1016/0142-727X(94)90015-9.

[9] A.K. Baranwal, R.P. Chhabra, Effect of fluid yield stress on natural convection from horizontal cylinders in a square enclosure, Heat Transfer Eng. 38 (6) (2017) 557–577, https://doi.org/10.1080/01457632.2016.1200373.

[10] L. Mishra, R.P. Chhabra, Combined effects of fluid yield stress and geometrical arrangement on natural convection in a square duct from two differentially heated horizontal cylinders, J. Therm. Sci. Eng. Appl. 12 (2020) 1, https://doi.org/10.1115/1.4044429.

[11] M. Corcione, et al., Buoyancy-induced convection from a pair of heated and cooled horizontal circular cylinders inside an adiabatic tilted cavity filled with alumina/water nanofluids, Int. J. Numer. Meth. Heat Fluid Flow (2019), https://doi.org/10.1108/HFF-01-2019-0023.

[12] Y. Ma, M. Jamiatia, A. Aghaei, M. Sepehrirad, A. Dezfulizadeh, M. Afrand, Effect of differentially heated tubes on natural convection heat transfer in a space between two adiabatic horizontal concentric cylinders using nano-fluid, Int. J. Mech. Sci. 163 (2019) 105148, https://doi.org/10.1016/j.ijmecsci.2019.105148.

[13] C.J. Ho, G.N. Sou, C.M. Lai, Effects of a flow mode transition on natural convection heat transfer in a heat tracing enclosure, Proc. Inst. Mech. Eng. Part E: J. Process Mech. Eng. 233 (3) (2019) 489–499, https://doi.org/10.1177/0954408918764456.

[14] F. Garoosi, F. Hoseininejad, M.M. Rashidi, Numerical study of natural convection heat transfer in a heat exchanger filled with nanofluids, Energy 109 (2016) 664–678, https://doi.org/10.1016/j.energy.2016.05.051.

[15] A. Quintino, E. Ricci, E. Habib, M. Corcione, Natural convection from a pair of differentially-heated horizontal cylinders aligned side by side in a nanofluid-filled square enclosure, Energy Procedia 126 (2017) 26–33, https://doi.org/10.1016/j.egypro.2017.08.050.

[16] A. Quintino, E. Ricci, E. Habib, M. Corcione, Natural convection from a pair of differentially-heated horizontal cylinders aligned side by side in a nanofluid-filled inclined square enclosure, J. Nanofluids 7 (6) (2018) 1290–1296, https://doi.org/10.1166/jon.2018.1542.

[17] F. Garoosi, F. Hoseininejad, Numerical study of natural and mixed convection heat transfer between differentially heated cylinders in an adiabatic enclosure filled with nanofluid, J. Mol. Liq. 215 (2016) 1–17, https://doi.org/10.1016/j.molliq.2015.12.016.

[18] F. Garoosi, F. Hoseininejad, M.M. Rashidi, Numerical study of heat transfer performance of nanofluids in a heat exchanger, Appl. Therm. Eng. 105 (2016) 436–455, https://doi.org/10.1016/j.applthermaleng.2016.03.015.

[19] P. Nithiarasu, K.N. Seetharamu, T. Sundararajan, Natural convective heat transfer in a fluid saturated variable porosity medium, Int. J. Heat Mass Transf. 40 (16) (1997) 3955–3967, https://doi.org/10.1016/S0017-9310(97)00008-2.

[20] L. Mishra, R.P. Chhabra, Natural convection in power-law fluids in a square enclosure from two differentially heated horizontal cylinders, Heat Transfer Eng. 39 (10) (2018) 819–842, https://doi.org/10.1080/01457632.2017.1338856.

[21] C.J. Ho, G.N. Sou, C.-M. Lai, Transient heat transfer between two horizontal pipelines in a heat tracing enclosure, Energies 12 (8) (2019) 1440, https://doi.org/10.3390/en12081440.

[22] J.T. Hu, S.J. Mei, Combined thermal and moisture convection and entropy generation in an inclined rectangular enclosure partially saturated with porous wall: nonlinear effects with Soret and Dufour numbers, Int. J. Mech. Sci. 199 (2021) 106412, https://doi.org/10.1016/j.ijmecsci.2021.106412.

[23] G. Nammi, D.K. Deka, S. Pati, L. Baranyi, Natural convection heat transfer within a square porous enclosure with four heated cylinders, Case Stud. Therm. Eng. 30 (2022) 101733, https://doi.org/10.1016/j.csite.2021.101733.

[24] A.A. Mohamad, Lattice Boltzmann method: fundamentals and engineering applications with computer codes, Springer Science & Business Media, London. (2011), https://doi.org/10.1007/978-1-4471-7423-3.

[25] E.-B. Lahmer, Y. Admi, M.A. Moussaoui, A. Mezrhab, Improvement of the heat transfer quality by air cooling of three-heated obstacles in a horizontal channel using the lattice Boltzmann method, Heat Transfer. 51 (2022), https://doi.org/10.1002/htj.22481.

[26] J. Kozeny (1927). Ueber kapillare Leitung des Wassers im Boden. Sitzungsber Akad. Wiss., Wien, *Royal Academy of Science, Vienna, Proc. Class* I 136(2a): 271-306. https://cir.nii.ac.jp/crid/1571417124968987776.

[27] P.C. Carman, Fluid flow through granular beds, Trans. Inst. Chem. Eng. 15 (1937) 150–166. https://cir.nii.ac.jp/crid/1570009749208809856.

[28] P.C. Carman, Flow of gases through porous media, Butterworths Scientific Publications, New York, 1956 https://cir.nii.ac.jp/crid/1573668923914024960.